Dosimetric Properties of Thermoluminesent Material $BaSO_4$: Eu

Devendra Joshi

Thesis submitted for the degree of

Master in Biological and Medical Physics

60 credits

Department of Physics

The Faculty of Mathematics and Natural Science

UNIVERSITY OF OSLO

Spring 2022

Dosimetric Properties of Thermoluminesent Material $BaSO_4$: Eu

Devendra Joshi

Dosimetric Properties of Thermoluminesent Material $BaSO_4$: Eu

http://www.duo.uio.no/

Printed: Reprosentralen, University of Oslo

Contents

List of Figures

List of Tables

Abstract

The thermoluminescence dosimetry system consists of a radiation dosimeter with crystalline thermoluminescence material. When a thermoluminescence material is exposed to ionizing radiation, it absorbs the energy of radiation on it. When the material is heated, it emits photons from the crystal lattice, the intensity of which is proportional to the absorbed ionizing radiation.

In this project, thermoluminescence material as $BaSO_4 : Eu$ polycrystalline material was studied in order to test whether the material has properties for a good TL dosimeter material and can have the potential for radiation dosimeter applications. Nano-crystalline $BaSO_4$ activated by europium (Eu) was prepared by the coprecipitation method with the concentration of the dopant Eu at 0.5 mol%, at which it showed maximum thermoluminescence (TL) sensitivity. The material was irradiated by X-rays and Co-60 γ-rays. The dose range for X-rays was 0.01 Gy to 0.03 Gy and for γ -rays 0.1 Gy to 1 Gy. The x-ray voltages used are 100 kV, 160 kV, and 225 kV, while Co-60 γ-rays has an average energy of 1.25 MeV. A linear relationship was observed between the TL intensity and dose within the given dose range for both X-rays and Co-60 γ-rays. The TL sensitivity of the material was found to be almost identical at X-ray voltages of 100 kV and 225 kV. However, the TL sensitivity of 225 kV X-rays was observed to be 47 times higher than that for Co-60 γ-rays, which was very close to the theoretical calculated value of 41. Moreover, the sensitivity of 160 kV X-rays was found to be 63 times higher. This shows that nano-crystalline $BaSO_4 : Eu$ is highly dependent on photon energy.

The heating rate effect was observed for four different heating rates 5, 10, 15, and 20 K/s. A shift in TL peak temperature with increasing the heating rate and a linear relationship between heating rate with TL intensity was observed. The signal residuals

were found to increase with increasing heating rate. The fading of the phosphor was studied in the interval of five days for ten consecutive cycles in total of 50 days. The fading in the TL signal was observed to be less than 7 % for 50 days, indicating that material has very low fading. The reusability test showed that out of ten cycles, after the first cycle, there was decrease in TL intensity, but the signal remains almost constant for rest of the cycles. The phosphor was also studied with EPR dosimetry by irradiating it by 225 kV X-rays with doses of 1 to 3 Gy. A linear relation was observed between the material's EPR intensity and dose, although the EPR signal was complex and weak.

In conclusion, $BaSO_4 : Eu$ has high sensitivity, simple glow curve, a linear relationship between TL intensity and dose, good reusability and low fading which indicate the potential of the material for radiation dosimetry applications. Still, the photon energy dependence may limit the applicability for X-rays with energies below some hundred keV.

Acknowledgement

First of all, I would like to express my sincere gratitude to supervisors Prof. Eirik Malinen and Assoc. Prof. Nina Frederike Jeppesen Edin for their support and guidance throughout this work. I am grateful to Eirik for being motivational and supportive throughout this work. Thank you for being there every week with valuable suggestions, without which it was impossible to complete this thesis. I found myself very fortunate to work with a professor like him.

I would like to thank Ravikumar Nattudurai and Delmon Arous for their assistance and guidance. A special thanks to Ravikumar for being helpful, always ready to spend time in my need, and answering my questions.

I am grateful to the Biophysics and Medical Physics section for giving me a great working environment. In addition, I thank all the fellow students, employees, and highly devoted professors of this section.

I would like to express my thanks and immense graduate to my parents and wife for their continuous support and everlasting love. The work would be challenging during a pandemic without your unconditional support.

Last but not least, I would like to thank the Department of Physics, the University of Oslo, Norway, for providing quality education and excellent opportunity.

List of Symbols and Abbreviations

TLD	-	Thermoluminescence dosimeter
rpm	-	Revolution per minute
Eu	-	Europium
ρ	-	Density
SSD	-	Source to surface distance
TL	-	Thermoluminescence
RT	-	Radiotherapy
Gy	-	Gray
a.u.	-	Arbitrary unit
MeV	-	Mega electron volt
keV	-	Kiloelectron volt
mg	-	Milligram
RC	-	Recombination Center
K	-	Kelvin
τ	-	Mean lifetime
T_m	-	Peak or maximum temperature
k	-	Boltzmann constant
α	-	Alpha (Frequency factor)
p	-	Probability of escape
E	-	Trap depth
q	-	Heating rate

μ_e	-	Magnetic moment of electron
g	-	Lande's factor
B	-	Bohr magneton
h	-	Planck's constant
m_e	-	Mass of electron
B_0	-	Magnetic field intensity
EPR	-	Electron paramagnetic resonance
PM	-	Photomultiplier
EPD	-	Electronic personal dosimeter
KERMA	-	Kinetic energy released per unit mass
ν_{max}	-	Maximum frequency
V	-	Potential difference
DC	-	Direct current
CPE	-	Charged particle equilibrium
Kg	-	Kilogram
J	-	Joule
Z	-	Atomic number
ϵ_{tr}	-	Expectation value of energy transfer
Ψ	-	Energy fluence
Φ	-	Fluence
T	-	Kinetic energy
CSDA	-	Continuous slowing down approximation
μ	-	Attenuation coefficient
E_b	-	Binding energy
Co	-	Cobalt

Chapter 1

Introduction

"The study of physics is also an adventure. You will find it challenging, sometimes frustrating, occasionally painful, and often richly rewarding."

HUGH D. YOUNG

Radiation physics is the study of ionizing radiation and its interaction with matter and subsequent energy deposition. When living tissue absorbs ionizing radiation, chemical and biological changes can be seen. These changes may result in the immediate damage or death of the cells or genetic alterations. The extent of changes in the tissue depends upon the amount of energy absorbed in the form of ionization. An ionization is the liberation of an electron from an atom or molecule, and is the principal radiation damage [1].

In radiotherapy and diagnostic radiology utilizing ionizing radiation such as X-rays, it is important to estimate the absorbed dose in the patient from the radiation exposure. This is because use of ionizing radiation is strictly regulated, and accurate dosimetry is required to ensure that absorbed doses are within prescribed or allowed limits. A radiation dosimeter measures the amount of energy absorbed by its sensitive material from the incident radiation. A tissue equivalent dosimeter has an atomic

composition which is close to that of human soft tissue, meaning that the dosimeter absorbs the same, or approximately the same, amount of energy per mass as soft tissue. Different dosimeters and dosimeter materials may or may not be tissue equivalent, and it is generally challenging to fabricate good dosimeters. If the dosimeters are not tissue-equivalent, corrections to the dosimeter reading are required to determine the soft tissue dose [2]. Although radiation dosimetry has significant applications in several fields, we focus on its uses in radiotherapy and diagnostic radiology.

Radiation dosimeters essential devices for radiation workers to monitor their radiation exposure and when treating cancer patients in the clinics that need accurately delivered doses to avoid normal tissue toxicity or lack of tumor control. There are several methods and approaches to measure the absorbed dose depending on the purpose. For example, ionization chamber dosimetry, semiconductor dosimetry, chemical dosimetry, calorimetric dosimetry, film dosimetry, thermoluminescence dosimetry and etc. The different methods have their advantages or disadvantages. For an instant, ionization chambers are well known for accurate and precise measurements recommended for beam calibration. As they are active dosimeters, they give instant or real-time dose measurements. On the other hand, they have some disadvantages as well. They required a high voltage supply and long cables. Moreover, large corrections are needed for high-energy beam dosimetry[3].

Thermoluminescence dosimeters (TLDs) have great advantages for personal and environmental dosimetry.They work on the principle that when ionizing radiation passes through them, it is absorbed by TLDs. When it is heated in a TLD reader, it emits light proportional to the amount of ionization radiation absorbed. These dosimeters are used in radiotherapy and diagnostic radiology because of their small size, easy preparation, accuracy, cost effectiveness and ease of handling. The improvements in technology made TLD more precise in e.g. use for organ dose measurement and intracavity measurements. TLD is found to be very convenient for patients and radiation workers to monitor cumulative doses [4].

The standard TL dosimeters that are available nowadays have some limitations;

that is, they do not possess all the characteristics for an optimal TL dosimeter such as high sensitivity, simple glow curve, reusability, tissue equivalence, linear dose response for wide range of doses, energy independence, negligible fading, non-toxicity and easy handling [5]. None of the existing standard TL dosimeters have all of the above characteristics. For example, LiF:Mg,Ti (TLD-100) is used as a standard TL dosimeter; it is tissue equivalent but has poor sensitivity. LiF:Mg,Cu,P (TLD-100H) is very sensitive to ionizing radiation, but it is also very sensitive to heat treatments, and it cannot be reusable without proper heat treatment. CaSO4:Dy (TLD-900) is very sensitive and reusable but it is energy-dependent [6]. Moreover, another problem with the TL dosimeter is the TL saturation and non-linear response at high doses [7]. Thus, there is a search for either the new TL dosimeter with better TL characteristics or to improve the existing TLDs by adding different types of dopants and their concentrations [8].

The present study aims to test the TL characteristics of $BaSO_4$ doped with europium as impurity. The project starts with preparing nanocrystalline $BaSO_4 : Eu$ material with the goal to optimize the concentration of the impurity. The TL characteristics are studied by irradiating the material with X-rays and γ-rays, where the lack of tissue equivalence also is investigated. The study main goal is to identify whether the material has potential for the clinical dosimetry applications.

Chapter 2

Background

Protons give an atom its identity, electrons its personality.

BILL BRYSON

2.1 Ionizing radiation

The following part is based on the chapters 3, 7, 8 and 9 of book "Introduction to Radiological Physics and Radiation Dosimetry" [9] and chapter 7 of book " Ionizing radiation effects and application." [10].

The radiation responsible for ionizing the atoms or molecules in a matter is called ionizing radiation. All radiations are not ionizing, but if the kinetic or quantum energy is sufficiently high, electrons can be ejected from atoms or molecules. For instance, electromagnetic radiations (like X-rays,γ-rays), neutron beams, and some heavy particles like beta particles, alpha particles, lithium ions, carbon ions, etc., are ionizing radiations. These types of radiation have different properties and have different ionizing powers.

Depending upon the interaction of ionizing radiation to the matter, they are divided into two types-directly ionizing radiation and indirectly ionizing radiation. Directly ionizing radiation is the radiation that interacts with the matter directly by Coulomb's force. Due to this force, there is an attraction or repulsion between the radiation and electrons from atoms or molecules of matter, for example, energetic electrons, positrons, protons, alpha particles, and heavy ions. Indirectly ionizing radiation is defined as the radiation interacting with matter indirectly and is responsible for releasing charge particles from atoms or molecules, which is then responsible for nuclear transformation. They consist of uncharged particles. An example of indirectly ionizing radiation is photons above 10 keV (X-rays and γ-rays) and all neutrons.

The different kinds of interaction phenomenon which takes place when electromagnetic and charged particle interacts with matter, is explained below.

2.1.1 Interaction of electromagnetic radiation in matter

When photons pass through matter, there is a given probability that the photon will interact. If an interaction takes place, the photon will lose all or a substantial fraction of its quantum energy. There are mainly three types of photon interactions that take place in matter:

1. Compton effect
2. Photoelectric effect
3. Pair production

These types of interactions are most important in the transfer energy to electrons and thus in a matter. Besides these interactions Rayleigh and photonuclear interactions can occur but these two interactions are less significant. The Rayleigh scattering is

elastic scattering and has no energy loss. Photonuclear interactions are only significant when a photon have energy above a few MeV.

The photoelectric effect is dominant at the low photon energies and high atomic number of the absorbers, the Compton effect takes over at medium energies and pair production is at higher energies. The different type's interaction depending upon the energy of ionizing radiation and the atomic number of absorbers is shown in figure [2.1].

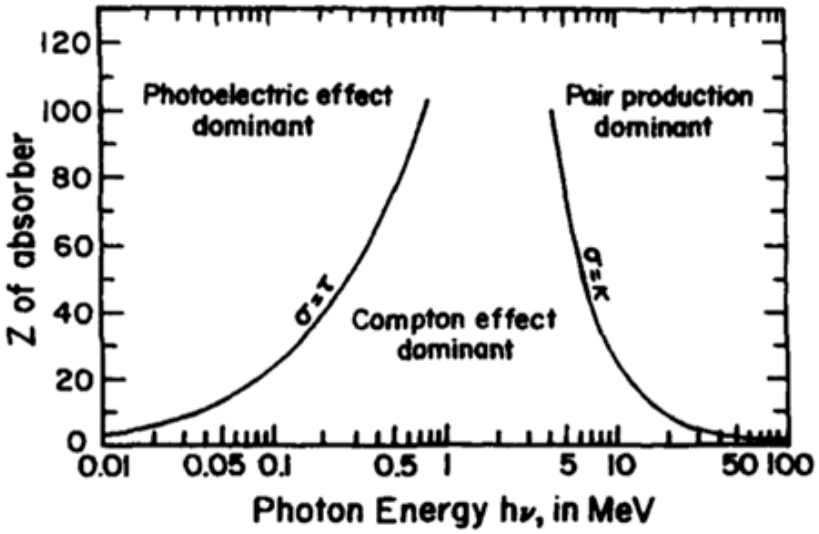

Figure 2.1. Relative importance of three types of interactions with respect to photon energy and atomic number Z of absorber [9].

Compton effect

When the incident photon collides with the stationary electron, some of the energy is absorbed by the electron. The electron moves away with some angle θ, while the photon deviates from the original direction by an angle Φ. The wavelength of the scattered photon is greater than the incident photon. This phenomenon is called the Compton Effect. The phenomenon of Compton Effect is shown in figure [2.2].

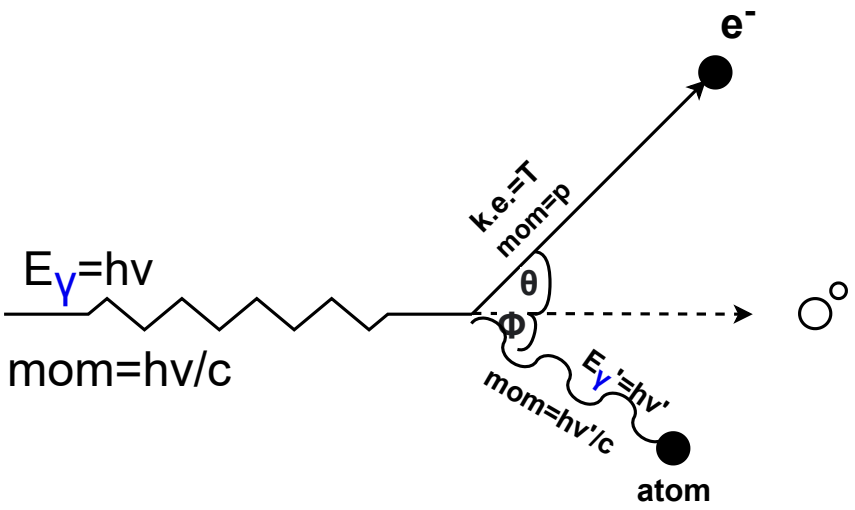

Figure 2.2. Kinematics of Compton effect. Figure adapted from Ref: [9].

Photoelectric effect

The photoelectric effect is dominant at the low photon energies and high atomic number of the absorbers. When the fast-moving photon beam strikes the tightly bound

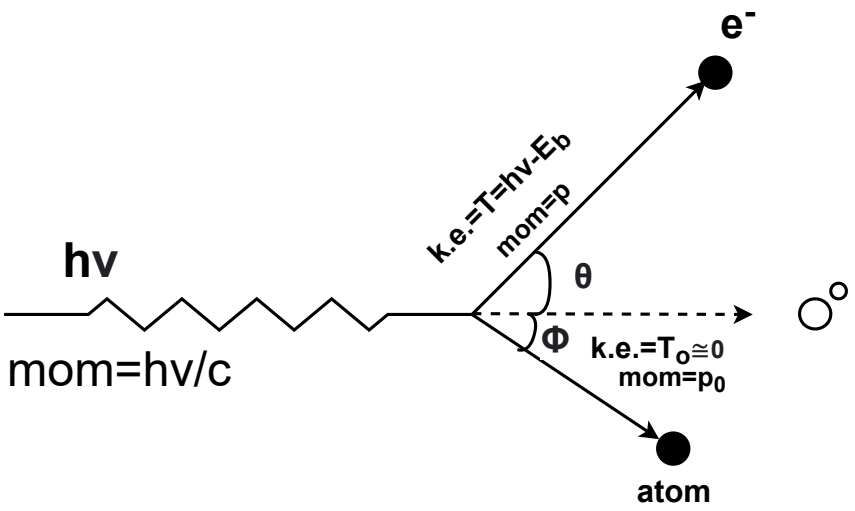

Figure 2.3. Kinematics of Photoelectric effect. Figure adapted from Ref: [9].

electron of the inner shells of an atom, the electron is ejected. If the incident energy of photons is greater than the binding energy of electrons, the emitted electrons move with an energy equal to the difference between incident energy and binding energy. Mathematically the kinetic energy of emitted electrons is given by equation [2.1].

$$T = h\nu - E_b \tag{2.1}$$

Where E_b is the threshold or the bound energy of electrons.

The electrons are scattered with an angle θ relative to the direction of the incident photons as shown in figure [2.3]. Since the photon has been absorbed, there is no scattered photon to conserving momentum as in the Compton Effect case. In the case of the photoelectric effect that role is assumed by the atom from which the electron was removed. Although its kinetic energy $T_a \approx 0$, its momentum p_a cannot be negligible.

Pair production

Pair production is an absorption process in which a photon disappears and gives rise to an electron and positron. The incident photon gives all its quantum energy in the creation of electron-positron pair. The rest mass-energy of the electron-positron pair is 1.02 MeV, so this amount of minimum energy (Threshold energy) is required for photons to produce electron-positron pair. If this energy is less than threshold energy, then no pair is produced and if the energy is higher the electron-positron pair is created with some kinetic energy.

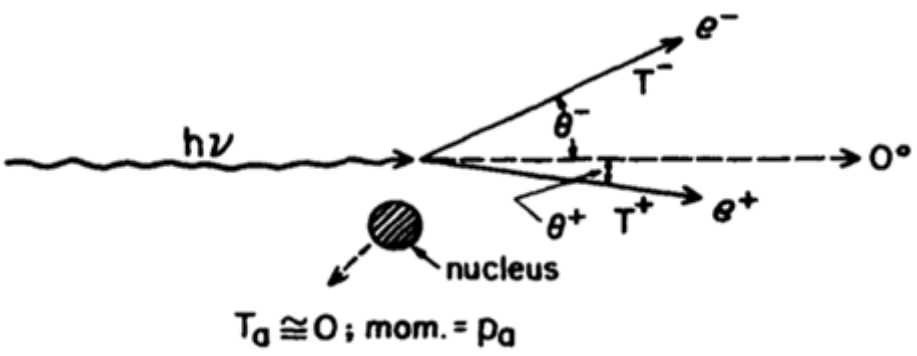

Figure 2.4. Kinematics of Pair production [9].

The pair production is only possible in the presence of a nucleus to carry off the excess momentum, it contributes to the conservation of momentum for the process to occur.

Pair production in the Coulomb force field of an atomic nucleus is shown in figure [2.4].

2.1.2 Exponential attenuation

The concept of exponential attenuation is primarily relevant to indirectly ionizing radiations, which lose their energy in relatively large interactions than the charge particles, which undergo small many interactions and gradually lose their kinetic energy. The photons or neutrons have high probability to pass straight to a high extent in a matter without losing any energy, however the charged particle always lose some or all its energy.

Consider an ideal case of exponential attenuation in which the particle is either completely absorbed producing no secondary radiations or passes straight unchanged in energy or direction through a matter. Let us assume a monoenergetic beam consists of large number N_0 of uncharged particles incident on a flat plate of thickness L as shown in figure [2.5]. Suppose μ be the probability that the incident particle interacts in a unit thickness of material.

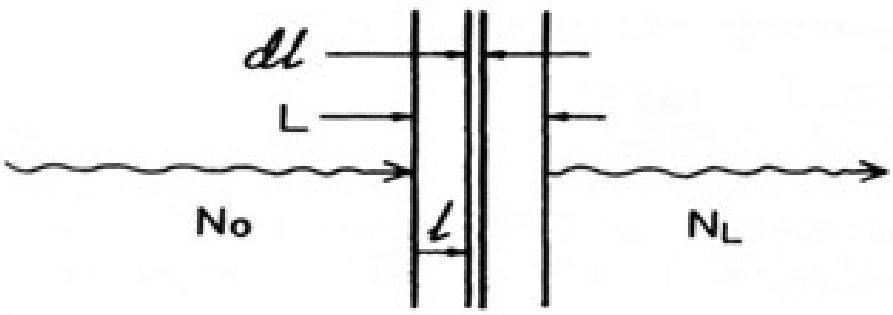

Figure 2.5. Simple exponential attenuation [9].

Then the probability that it will interact in an infinitesimal thickness dl is μdl. If N be the number of particles incident upon dl, then change in the number of particles dN due to absorption is given by

$$dN = -\mu N dl \tag{2.2}$$

Where μ is measured in the units of cm^{-1} or m^{-1}. Now, the fractional change in number of particles due to absorption in dl is

$$\frac{dN}{N} = -\mu dl \tag{2.3}$$

Integrating over the depth from 0 to and corresponding number of particles from N_0 to N_L, then we have

$$\begin{aligned} \int_{N_0}^{N_L} \frac{dN}{N} &= -\int_0^L \mu dl \\ lnN_L - lnN_0 = ln\frac{N_l}{N_0} &= -\mu L \\ \frac{N_L}{N_0} &= e^{-\mu L} \end{aligned} \tag{2.4}$$

This is the law of exponential attenuation. The quantity is called the linear attenuation coefficient. It describes the fraction of photons that is absorbed per unit length of the material. If linear attenuation coefficient is divided by the density of attenuating medium, mass attenuation coefficient is obtained. The mass attenuation coefficient μ/ρ is measured in cm^2/g or m^2/kg.

2.1.3 Charged particle interaction with matter

When the charged particles interact with matter, they lose their energy differently from that of uncharged radiation. Charged particles may interact through Coulomb's force, so they will almost continuously interact with electrons or the nuclei and thereby loses energy, which is called Continuous Slowing Down Approximation (CSDA). The probability for no interaction is zero when a charged particle passes through matter. It is possible to predict how far the charged particle can penetrate through matter roughly by using a common path length traced out by these particles of given type and energy in a specific medium. The charge particles undergo large number of interactions, and they go to slowing down. The path length tends to the expectation value that is a mean of large number of identical particles. That expectation value is called the range.

I. Types of charge particle interaction with matter

The interaction of the charged particle with matter can be classified in terms of the relative size of the impact parameter and the radius of the atom. It is convenient to classify three types of interactions that can happen between matter and charged particle.

Soft collision b»a

When a charged particle passes a considerable distance from an atom, the particles Coulomb fields affect the atom as a whole and excites it to a higher energy state, and sometimes ionizes it by ejecting the valence electron as shown in figure [2.6]. The net effect is the transfer of a very small amount of energy (a few eV) to an atom in the absorbing medium.

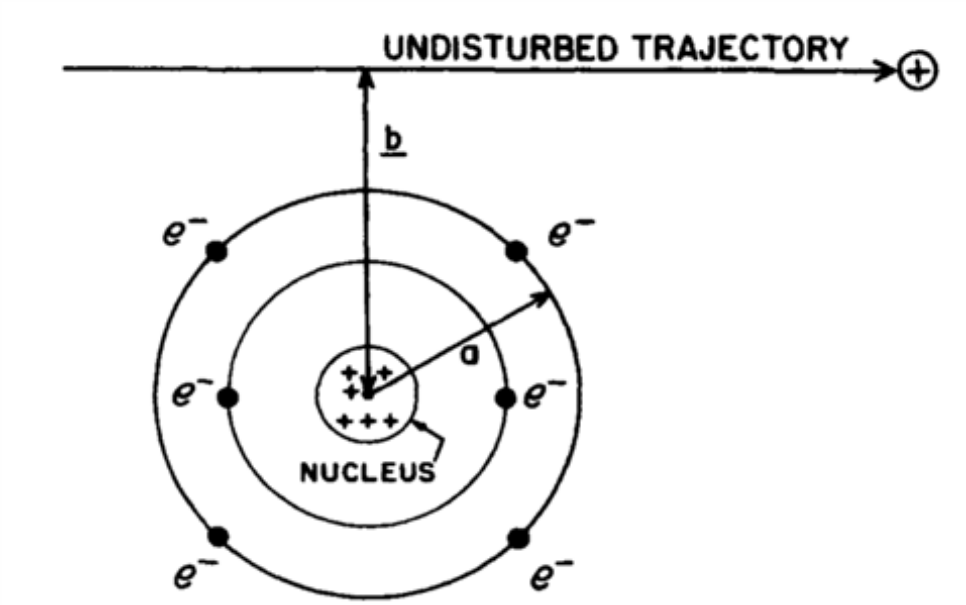

Figure 2.6. Charged particle interaction with matter, where a is classical atomic radius and b is impact parameter.[9].

Hard collisions b=a

When the impact parameter $'b'$ is close to that of atomic radius, then there is a great probability of interaction with a single atomic electron, which is then ejected from an atom with considerable energy called delta (δ) ray. These δ-rays deposit its kinetic energy along a separate track from that of the charged particle and have enough energy that they can undergo additional Coulomb force interactions of their own. The probability for the hard collisions depends upon the nature of the incident particle.

Coulomb-force interactions with the external nuclear field b«a

When the impact parameter is very smaller than atomic radius, charged particle interacts with the nucleus. When the charged particle interacts with nucleus by a Coulomb force, it gets deflected from its path without transferring noticeable amount of energy to it. About 2-3 % of the interaction of the electron is scattered elastically and does not emit X-ray photons or excite the nucleus. Another small number of interactions, electron passes near the nucleus, get deflected from their path there by

losing a significant amount of incident energy, an inelastic radiative interaction occurs in which an X-ray photon is emitted. These X-rays are called bremsstrahlung.

II. Nuclear interaction by heavy charged particle

When the nuclear interactions occur by a heavy charged particle of the high kinetic energy and impact parameter less than nuclear radius, an inelastic collision takes place. The highly excited nucleus decays from its excited state by the emission of evaporation particles and γ-rays. The amount of absorbed dose is changed when nuclear interactions are present since fraction of the kinetic energy that is deposited as local excitation and ionization is carried away by neutrons and γ-rays.

2.1.4 Stopping power

The stopping power is defined as the expectation value of the rate of the kinetic energy $'T'$ loss per unit length $'x'$ of the charged particle $(\frac{dT}{dX})$, in a medium having atomic number Z. It is measured in MeV/cm or J/m. If the stopping power is divided by density of the absorbing medium, mass stopping power is obtained $(\frac{dT}{\rho dX})$. It is measured in $MeVcm^2/gm$ or Jm^2/kg. When a charged particle interacts with a matter, it slowly stops after traversing some path length as the charged particle loses its kinetic energy due to interaction with atoms or molecules of a matter. Depending on the type of charged particle interaction, the stopping power is divided into two types- collision stopping power and radiative stopping power. The collision stopping power results from the interactions of charged particles with orbital electrons of an atom, as in the case of soft and hard collisions. The radiative stopping power results from the interaction of charged particles with the atomic nuclei in the case of nuclear interactions, as discussed above.

2.2 Dosimetry and dosimetric quantities

The following section is based on chapter 2 of "Introduction to radiological physics and radiation dosimetry" [9].

In radiology, dosimetry is the quantitative measurement of the amount of energy deposited in a matter directly or indirectly by ionizing radiation. To describe the amount of dose deposited in a matter several dosimetric quantities are required and explained below.

2.2.1 Fluence

The fluence can be defined as the expectation values of number of rays (photon quanta) or particles striking per unit cross-sectional area. If dN_e be the number of rays striking area da of a sphere of great circle, then fluence is given by

$$\Phi = \frac{dN_e}{da} \tag{2.5}$$

It is expressed in units of m^{-2} or cm^{-2}.

When radiation passes through matter, the fluence varies due to the absorption, scattering and the creation of new particles.

2.2.2 Fluence rate

Fluence rate or the flux density is defined as time rate of change of fluence during the infinitesimal time interval.

$$\phi = \frac{d\phi}{dt} = \frac{d}{dt}\left(\frac{dN_e}{da}\right) \tag{2.6}$$

Where $d\phi$ is the increment of fluence during the infinitesimal time interval dt. It is usually measured in $m^{-2}\ s^{-1}$ or $cm^{-2}\ s^{-1}$.

2.2.3 Energy fluence

This term considers of all the energies of individual radiations. Suppose R be the expectation value of the total energy carried by all $N_e$rays of finite sphere of having great circle of area da. Then energy fluence is given by

$$\Psi = \frac{dR}{da} \tag{2.7}$$

For mono-energetic radiation having energy E, we can write $R = EN_e$. Thus, $\psi = E\phi$. It is expressed in the units of Jm^{-2} .

2.2.4 KERMA

The quantity KERMA (Kinetic energy released per unit mass) is used to describe the energy dissipation by indirectly ionizing radiation, that is energy transfer to charged particles. It is a nonstochastic quantity. KERMA is defined as expectation value of energy transferred to charged particles per unit mass at the point of interest, including the radiative loss. It is given by

$$K = \frac{d\epsilon_{tr}}{dm} \tag{2.8}$$

Where $\epsilon_{tr} = (R_{in})_u + \sum Q$, is the expectation value of the energy transferred in the finite volume V during some time interval. It can be expressed in units of JKg^{-1}. For monoenergetic photons, the KERMA at a point is related to energy fluence by the relation

$$K = \Psi\left(\frac{\mu_{tr}}{\rho}\right)_{E,Z} \tag{2.9}$$

Where $(\mu_{tr})E, Z$ is the mass energy transfer coefficient which is characteristics of photon energy E and atomic number Z of the matter. It is defined as the mean fraction of the energy transferred to a charged particle per unit length. It is measured in units of m^{-1}. ρ is the mass density measured in kgm^{-3}. The KERMA includes the kinetic energy received by charged particles which is used by electrons in collision or radiative interactions. So,

$$K = K_c + K_r \tag{2.10}$$

Where K_c and K_r is the collision and radiative KERMA respectively.

For neutrons $K = K_c$ as K_r is relatively very small. The net energy transfer for a volume V is defined by

$$\epsilon^n_{tr} = (R_{in})_u - (R_out)^{nonr}_u - R^r_u = \epsilon_{tr} - R^r_u \tag{2.11}$$

Where R_u is the radiant energy emitted as radiative losses by charged particles in volume V.

Now we can define K_c at a point as

$$K_c = \frac{d\epsilon^n_{tr}}{dm} \tag{2.12}$$

Where ϵ^n_{tr} is the expectation value of net energy transferred in the finite volume V in some time interval (excluding the radiative loss and the energy passed from one charged particle to another).

For monoenergetic photons K_c is related to energy fluence by energy and material dependent coefficient $\left(\frac{\mu_{en}}{\rho}\right)_{E,Z}$ called mass energy absorption coefficient by

$$K_c = \Psi \left(\frac{\mu_e n}{\rho} \right)_{E,Z} \tag{2.13}$$

The radiative KERMA is simply the difference between K and K_c.

2.2.5 Absorbed dose

Absorbed dose is defined as the expectation value of energy imparted to matter per unit mass at a point.

$$D = \frac{d\epsilon}{dm} \tag{2.14}$$

The energy imparted by ionization radiation to matter of mass m and finite volume is given by

$$\epsilon = (R_{in})_u - (R_{out})_u + (R_{in})_c - (R_{out})_c + \sum Q \tag{2.15}$$

Where

- $(R_{in})_u$ = radiant energy of uncharged particle entering volume V
- $(R_{out})_u$ = radiant energy of uncharged particles leaving volume V without radiative loss.

- $(R_{in})_c =$ radiant energy of the charged particles entering volume V.
- $(R_{out})_c =$ radiant energy of charged particles leaving V.
- $\sum Q =$ net energy derived from rest mass.

Absorbed dose is expressed in the same units as of KERMA that is Jkg^{-1}.

Both the absorbed dose and KERMA seems similar, but they are different. KERMA is only defined for indirectly ionizing radiation, and it represents the amount of energy transferred in finite mass of certain volume by the initial interaction of indirectly ionizing radiation. However, absorbed dose is relevant for all types of radiations.

In case of Charged Particle Equilibrium (CPE), the number of charged particle of given type entering in a volume V equals to the number of charged particle leaving it. So, at CPE,

$$(R_{in})_c = (R_{out})_c \tag{2.16}$$

Hence,

$$\epsilon = (R_{in})_u - (R_{out})_u + \sum Q = \epsilon_{tr}^n \tag{2.17}$$

Then absorbed dose is equal to collision KERMA and is given by

$$D = \frac{d\epsilon_{tr}^{n}}{dm} = K_c = \Psi \left(\frac{\mu_{en}}{\rho} \right)_{E,Z} \tag{2.18}$$

2.3 X-rays and X-ray production

X-rays are the very short wavelength radiations produced when a fast-moving electron beam Impinges a heavy target. They are electromagnetic waves that ionize the atoms or molecules of the matter through which they pass. The intensity of X-rays produced depend upon the accelerating potential difference applied between the anode and cathode.

The cathode and anode are placed inside an evacuated chamber (to avoid oxidation and corrosion) at two opposite sides. The cathode filament is made up of a metal (Tungsten) having a high melting point and a high atomic number and the anode as a target is also a heavy metal having high melting point. Further, the anode is joined with a cooling system to take out the heat generated in the anode after the bombardment of electrons. The anode and the cathode are the connected through high voltage potential. The energy of X-rays produced depends upon the potential difference applied between two electrodes. More than 90 % of the incident energy of electrons is converted into heat energy after striking with the target.

When a cathode filament is heated by a DC current, the electrons are emitted from the cathode by the process of thermionic emission. The number of electrons released from the filament is directly proportional to the current flowing in the filament up to some limits. The anode as a target is set at a positive potential on the other side. The high potential difference set up between the anode and cathode accelerates the emitted electrons towards the anode. When these fast-moving electrons strike the target, the X-rays are produced.The production of X-rays can as shown in the figure [2.7]. Due to the continuous bombardment of electrons with anode, it gets heated and is cooled down

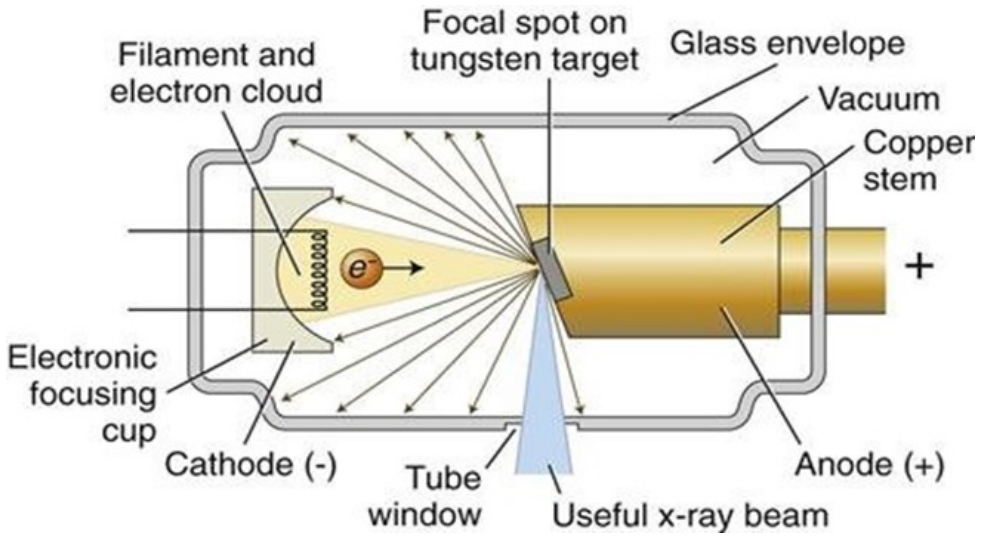

Figure 2.7. Schematic diagram of x-ray production[11].

by the oil for the heat conduction. Let V be the potential difference applied between two electrodes, then the kinetic energy gained by electron is

$$E = eV \tag{2.19}$$

Where e is the basic charge of the electron. When these electrons strike to a target X-ray are produced. If ν_{max} is the maximum frequency of the X-rays emitted, then we can write

$$h\nu_{max} = eV \tag{2.20}$$

Where h is the Planck's constant.

The energy of X-rays depends upon the distance of the electron that travel from the nucleus. If the electron approaches close to the nucleus, the kinetic energy lost by

electron is high thus the energy of X-rays produced is higher and vice versa.

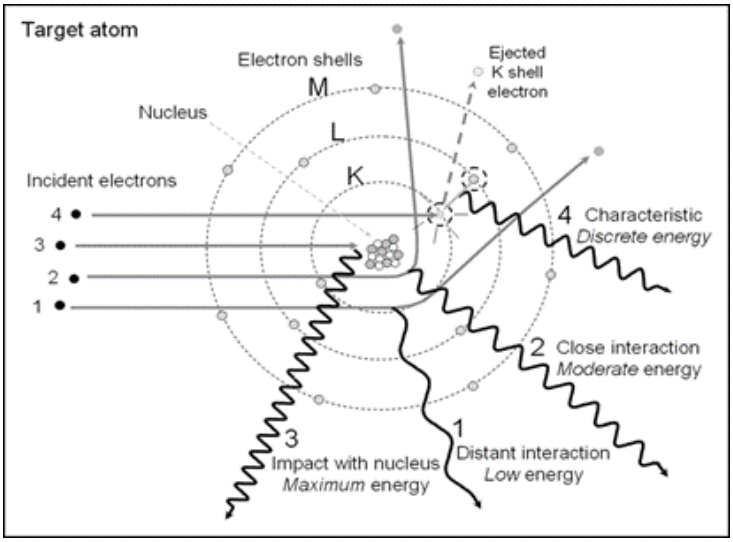

Figure 2.8. Schematic diagram of bremsstrahlung. In the figure four different beams striking with an atom: beam 1 close to nucleus and gets deflected by small extent producing low energy bremsstrahlung, Beam 2 very close to nucleus highly deflected producing high energy photons, Beam 3 strikes with nucleus producing maximum energy photons, beam 4 strikes with orbital electron thereby producing characteristics photons [11].

X-rays can be produced by means of two mechanisms. First, most X-rays can be produced by the bremsstrahlung process, as shown in figure [2.8]. In this process, when the fast-moving electrons strike the target, they pass close to the nucleus. Due to the electrostatic force between the electron beam and nucleus, it gets deflected. The deflection of the beam causes its kinetic energy to decrease, which is then converted into the energy of X-ray photons, which are called bremsstrahlung. The other mechanism is less common and is called characteristic X-rays production. They are produced when the fast-moving electron strikes the target and an electron is knocked out by it, the vacancy thus created is fulfilled by the electron from the high energy level. During this process, characteristic X-rays are produced. When the electron of K-shell is removed by the collision of an electron from cathode then the vacancy in the K-shell is fulfilled by an electron from L-shell with maximum probability thereby generation of characteristic k_α line. Similarly, if the vacancy in the K-shell is fulfilled by the electron from M-shell then the k_β line is generated. On the other hand, if the vacancy is created in the L-shell by collision, then electron from M-shell and N-shell jumps to fulfill that vacancy thereby generating of l_α and l_β lines. Generation of characteristic K and L lines depends upon the energy of incident electron beam, as high energy is required to remove an electron from K-shell than L-shell, so the spectrum of characteristic K-line

has larger peaks than L lines.

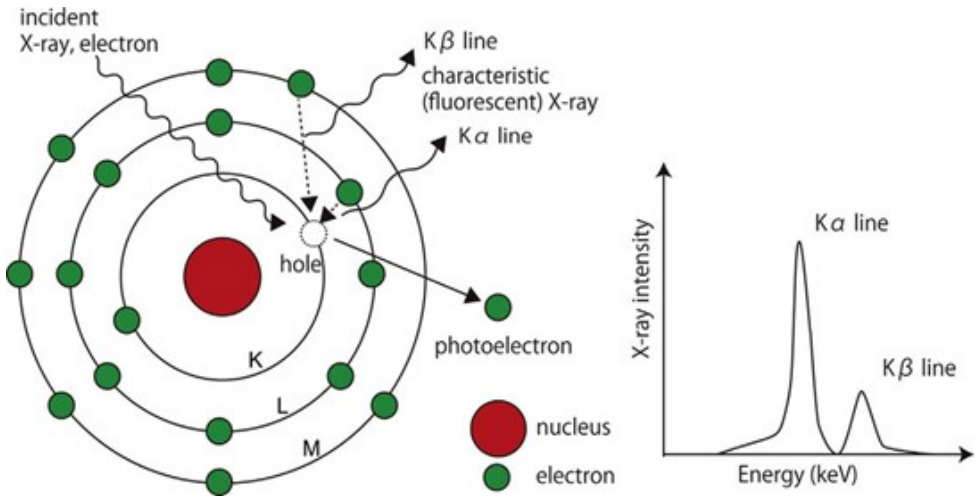

Figure 2.9. Schematic diagram of Characteristic x-rays production [12].

The bremsstrahlung is the dominant phenomenon by which most of the X-rays are produced. The characteristic X-rays give a line spectrum while the bremsstrahlung gives a continuous spectrum. The X-ray spectrum can be shown in figure [2.10].

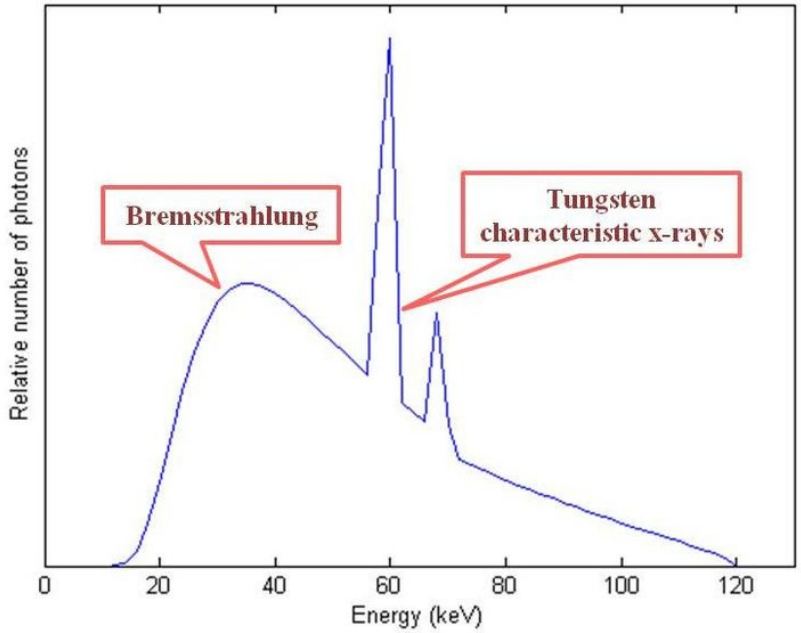

Figure 2.10. The X-ray spectrum showing both bremsstrahlung and characteristics X-rays [13].

2.4 Dosimeter

The following section is based on chapter 2 of “Introduction to radiological physics and radiation dosimetry” [9]. and chapter 3 of “Radiation oncology physics: A handbook for teachers and students" [14].

A dosimeter is a device that measures the absorbed dose deposited in its sensitive volume by ionizing radiation. The dosimeter can measure exposure, KERMA and equivalent dose and their rates either directly or indirectly. The following are the property of a good dosimeter.

- High Accuracy and precision
- Linearity
- Dose rate dependent
- Very high sensitivity to ionizing radiation
- Energy independence
- Directional dependence
- High Spatial resolution

There are mainly two types of dosimeters absolute and relative dosimeters. Absolute dosimeters do not require calibration and gives direct measurement of absorbed dose while in the relative dosimeters the radiation induced signals cannot be directly converted to dose. For the later, calibration is needed. The examples of absolute dosimeters are ionization chamber, Electronic Personal Dosimeter (EPD), calorimetric dosimeter, Fricke dosimeter etc. and the examples of relative dosimeter are film dosimeter, EPR dosimeter, thermoluminescence dosimeter etc.

2.4.1 Ionization chamber

Ionization chambers are most widely used for precise measurement of dose in radiotherapy and are commercially available in variety of designs for different applications. They use the principle that when ionizing radiation is passed through some gas, it ionizes the gas and electrons are produced. In the ionization chamber the gas is placed between two electrodes at high potentials (some hundred volts). Due to the presence of an electric field, the liberated electrons are collected at the positive terminal. The electrometer connected across it measures the current. The current is proportional to the ionization produced in the gas, thus measuring the dose of a given ionizing radiation as the number of ionization produced depends upon some external conditions like temperature, pressure, humidity, and the potential difference between the two electrodes. So, the calibration of the ionization chamber is done by considering the above-mentioned factors.

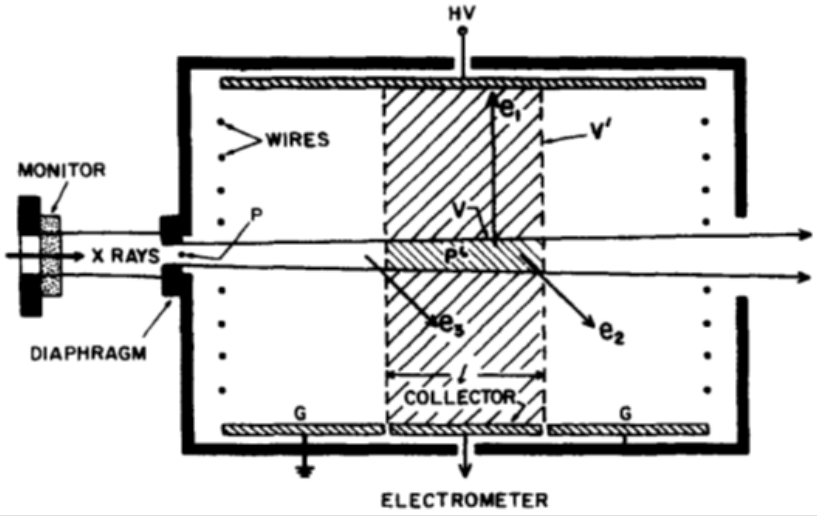

Figure 2.11. Schematic diagram of free-air ion chamber [9].

There are mainly of two types- free air ionization chamber (as shown in figure [2.11] and cavity ionization chamber (as shown in figure [2.12]. The free air ionization chamber requires nearly monodirectional beams aligned to pass perpendicular through the aperture while the cavity chamber measures multidirectional radiation fields. Cavity chambers can be used to measure dose of charged particles, photons as well as neutrons while free air chambers are exclusively designed for X-rays mainly below 300 keV.

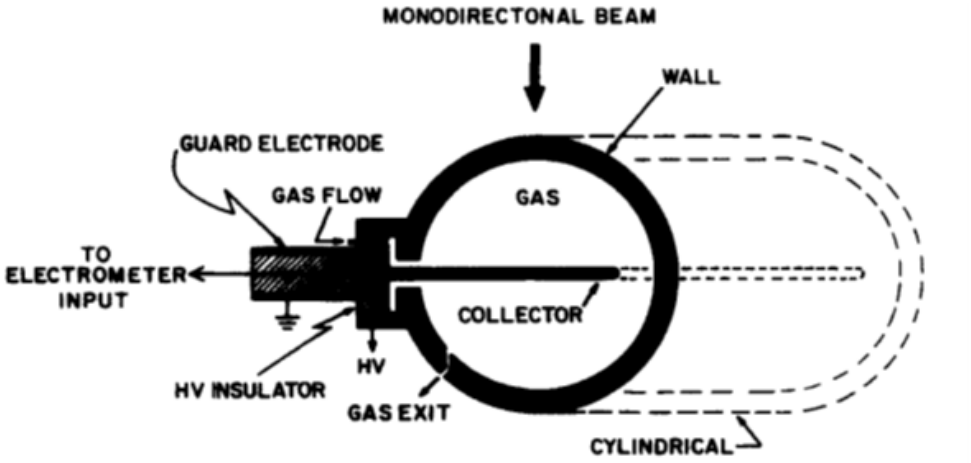

Figure 2.12. Schematic diagram of thimble type cavity chamber [9].

The cavity chamber is of different types according to the requirements like thimble-type chamber, flat cavity (extrapolation) chamber and transmission monitor chamber.

2.4.2 Thermoluminescence dosimetry

I. Thermoluminescence principle

Thermoluminescence is the phenomenon of emission of light from a dielectric material called phosphor, when a sample irradiated with ionizing radiation is heated. This phenomenon sometimes also called radiation induced thermally stimulated luminescence or radio thermoluminescence. The activators present in the phosphor provides two kinds of centers – Traps and Luminescence centers.

Traps are kinds of electric potential well where the electrons and holes are captured and held for a usefully long period of time. The luminescence centers are located at either the electron traps or the hole traps, which emit light when the electrons and holes recombine at such centers.

The phenomenon of thermoluminescence is shown in figure [2.13]. When a phosphor is irradiated with ionizing radiation, the ionization takes place at valence

band and electron is migrated towards conduction band, where it migrates towards electron trap. The hole left behind migrates to a hole trap. At room temperature, these traps are so deep in terms of potential difference that the electrons or holes cannot escape for long period of time.

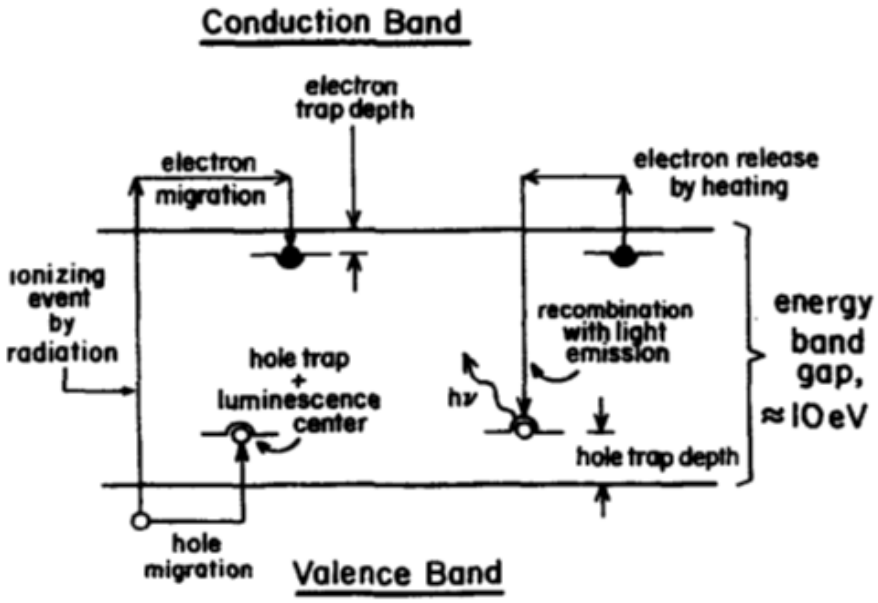

Figure 2.13. Thermoluminescence process showing two bands with traps and luminescence centers [9].

When the phosphor is heated after irradiation, the electrons released from electron trap move to the conduction band and migrates towards the hole trap which may be assumed to be a luminescence center. During this recombination process, the light photons are released. The amount of light emitted is proportional to the number of recombination events.

II. Randall-Wilkin's theory

The probability of escape of charge carriers per unit time at a temperature $T(K)$ were first described by Randall and Wilkins in 1945. The equation of probability of escape (first-order kinetics) is given by

$$P = \frac{1}{\tau} = \alpha e^{\frac{-E}{kT}} \tag{2.21}$$

Where is p is probability of escape per unit time, τ is the mean lifetime in the trap, α is called frequency factor, E is the energy depth of the trap (eV) and k is the Boltzmann's constant $(k = 8.62 \times 10^{-5} eV\, K^{-1})$.

If we assume α, E and k as constants, the from above equation it is evident that increasing T causes p to increase and τ to decrease. Thus, as the temperature increases from room temperature an increase in the rate of escape of trapped electrons will occur up to a certain temperature T_m the corresponding peak is called a glow peak as shown in the figure [2.14]. The multiple peaks in the glow curve are due to the presence of more than one trap depth E.

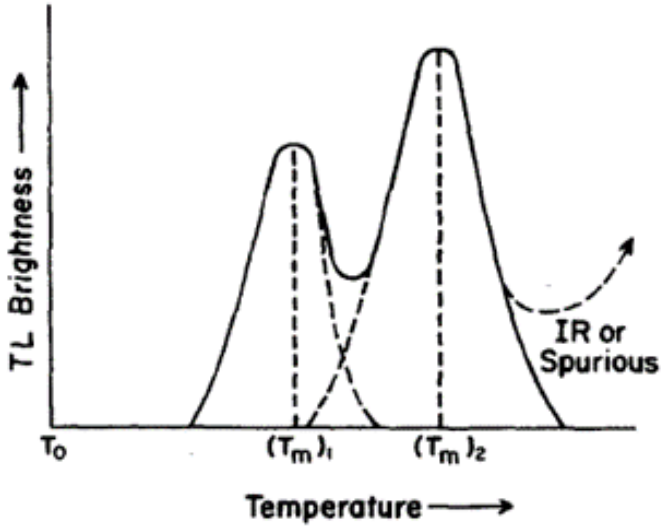

Figure 2.14. TL glow curve between temperature and TL brightness showing two peaks at two temperatures $(T_m)_1$ and $(T_m)_2$ [9].

The T_m is related to linear heating rate $q(K/s)$ is given by Randall- Wilkins theory by relation

$$\frac{E}{kT_m^2} = \frac{\alpha}{q} e^{\frac{-E}{kT_m}} \tag{2.22}$$

If we assume $\alpha = 10^9/s$ and $q = 1$ K/s, then from above equation $T_m = 498\ K/eV)E$. Hence T_m = 216 $^\circ C$ for $E = 1$ eV.

Since it is not obvious from equation [2.22], T_m increases gradually with q, so that at T_m = 248 $^\circ C$ at q = 5 K/s and 263 $^\circ C$ at q = 10 K/s for the same value of α and E.

III. Trap stability

The thermoluminescence phosphor is useful for dosimetric applications if phosphor traps depend on its independence of time and ambient conditions. Changes in the radiation sensitivity may occur if the traps migrate through the crystal and combine with others to form different configuration before irradiation. It is generally recommended that TL phosphors be treated uniformly and optimally with heat before and after use to achieve their best performance as a dosimeter. When a trap cannot hold charge carriers at room temperature following irradiation, this is called trap leakage. As a rule of thumb, a glow peak at around 200-225 $^\circ C$ is ordinarily found to have a small leakage at room temperature for practical dosimetry.

IV. TLD reader

The device which is used to heat a TLD phosphor and measure the thermoluminescence light signal is called TLD readers. The schematic diagram of TLD reader is shown in figure [2.15] below.

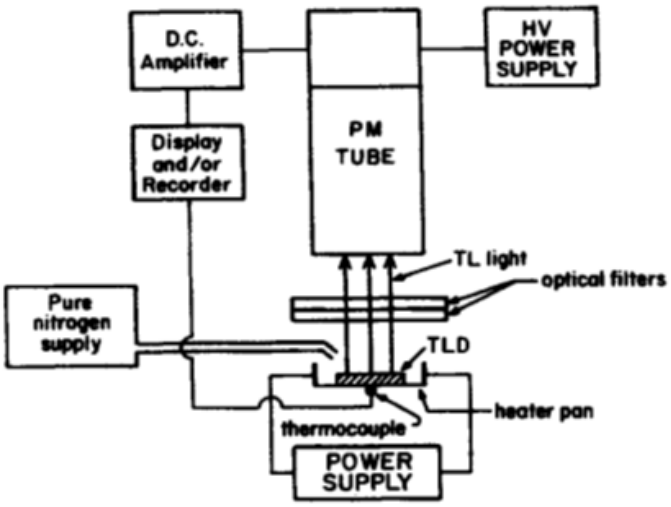

Figure 2.15. Schematic diagram of typical TLD reader [9].

The TLD phosphor is placed in the heater pan at room temperature and heater while the emitted light is measured with photomultiplier tube. Samples may be heated by means of Ohmically heated metal pans, by preheated N_2 gas, by an intense light spot generated by a projector lamp or laser or by any suitable method. The TLD reader heats the phosphor is heated rapidly through the unstable-trap region, which ignores light emission until a preset temperature is reached. Once the phosphor has been heated linearly or abruptly raised to a temperature sufficient to give off the glow peak of dosimetric interest, the measured total emitted-light sum is displayed as a charge or dose reading. Finally, the phosphor is heated further to $400^{\circ}C$ to release the remaining signals from deeper traps.

The heating-program is essential for reproducible dosimetry and constant light sensitivity since a given amount of TLD light output will always give the same reading. This requires a stable power supply no fatigue in the PM-tubes and a clean optical system (filters, mirrors, lenses light pipes and heater pan surface).

V. TLD phosphors

The TLD phosphors consist of a host crystal material that may contain one or more activators that may associated with the traps or luminescence centers or both. Different

phosphors contain different number of activators. Most of the radiation interactions are determined by the host crystal since activators are generally present in small amounts. The most commonly used TLD phosphors are $LiF:Mn, CaF_2:Mn, Li_2B_4O_7:Mn, CaSO_4:Mn$.

2.5 Electron Paramagnetic Resonance (EPR)

The following section is based on chapter 1 of "Introduction to electron paramagnetic resonance"[15].

EPR is the method of studying materials with unpaired electrons. It is therefore particularly useful for radicals. It is the technique based on the absorption of electromagnetic radiation in the microwave frequency region by a paramagnetic sample placed in a magnetic field. The absorption only takes place for certain frequencies and magnetic field combinations, depending upon the sample characteristics.

The electrons have both intrinsic charge and spin, they are rotating around their own axis. The electrons possess two spin states (parallel and antiparallel). Due to this spin, it possesses magnetic spin quantum number that is $m_s = \pm\frac{1}{2}$ for parallel and anti-parallel direction also called α and β states. The magnetic moment μ_e of electron is always associated with electron spin S angular momentum given by relation

$$\mu_e = g\mu_B S \tag{2.23}$$

Where g is a number called Lande's factor or simply g-factor. For electron $g = 2.002319$ and $\mu_B = \frac{-|e|h}{4\pi m_e} = -9.27 \times 10^{-24} JT^{-1}$, where m_e is the mass of electron, and h is Planck's constant. μ_B is the Bohr magneton ($\mu_B < 0$).

Due to the existence of magnetic moment associated with the electron spin, there is an energy separation between two states (α and β states) when an electron is present in the magnetic field.

If an electron is placed in the magnetic field , the splitting of the two energy states takes place. When the energy of electromagnetic radiation is equal to the energy difference between two energy states, a resonance takes place. That is at resonance

$$\Delta E = h\nu = g|\mu_B|S.B \tag{2.24}$$

The dot product reduces to a single term if the direction B coincides with one of the axes to which B and S are represented. In this case the above equation becomes

$$\Delta E = g|\mu_B|m_s B_0 \tag{2.25}$$

Where B_0 is the magnetic field intensity.

Since the electron have two components of spin (α and β), $m_s = \pm\frac{1}{2}$, so in the presence of magnetic field the splitting of electron spin energy is given by

$$\Delta E = \pm(\frac{1}{2})g|\mu_B|B_0 \tag{2.26}$$

Therefore, the splitting of electron energy level in two energy levels in the presence of magnetic field is called *Zeeman effect.* The splitting of energy level is shown in figure [2.16].

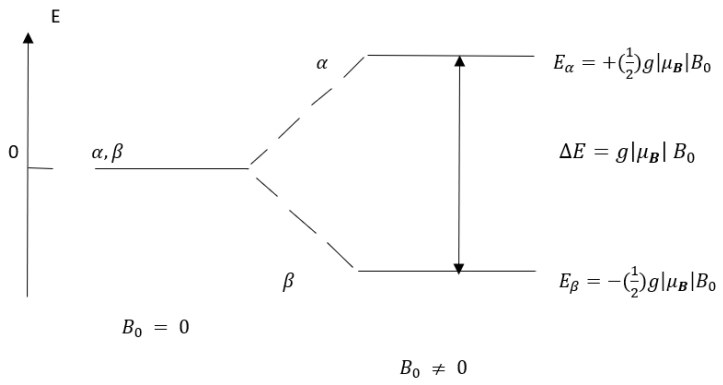

Figure 2.16. Splitting of energy levels of an electron in the presence of magnetic field. Figure adopted from [15].

Chapter 3

Materials and Methods

If your result needs a statistician then you should design a better experiment.

ERNEST RUTHERFORD

This chapter gives a detailed overview of different techniques and instruments that were used for this project work. The project work is mainly on dosimetry and thermoluminescence. So, the main concern is also based around thermoluminescence material, its preparation, TLD readers, detectors, and irradiation devices.

3.1 Material synthesis

The co-precipitation method is a classic and perhaps the simplest method for the synthesis of nanophosphor substances. Basically, this process involves the precipitation of salt (such as sulfates, nitrates, and chlorides) aqueous solutions by adding a base such as $(NH_4)_2SO_4, NaOH$, etc. Barium sulphate doped with europium (Eu^{3+}) were prepared by such a co-precipitation method. $BaCl_2$, $(NH_4)_2SO_4$ and $EuCl_2$ were used

as the starting ingredients. $BaSO_4 : Eu$ were prepared by dissolving $BaCl_2$ (Analytical grade 99.999% purity) with $EuCl_2$ and $(NH_4)_2SO_4$ in deionized water. When the two solutions were mixed together, the $BaSO_4 : Eu$ nanophosphors co-precipitated. The preparation of the sample and the precipitates of $BaSO_4 : Eu$ as shown in figure [3.1].

Figure 3.1. Left; The beaker containing $BaCl_2$ and deionized water solution placed in a magnetic stirrer. Right; the centrifuge tubes with the precipitate of $BaSO_4$ settled at bottom and clear solution of NH_4Cl at the top.

The clear liquid with chlorine content on the top of the precipitates was removed. The precipitates could settle down by centrifuge for 15 minutes with 1000 rpm. The precipitates were then washed and centrifuged five times with de-ionized water until the water in the beaker becomes neutral. After the precipitates were dried in hot air at $100^{\circ}C$ for 1 hour in a nitrogen atmosphere. Various samples of $BaSO_4 : Eu$ nanophosphors were synthesized by varying the europium concentration from 0.3, 0.5, 1, 1.5, 2, 2.5 and 3 mol% gave optimum sensitivity. The concentration of 0.5 mol% of europium activated $BaSO_4$ exhibits higher yielding maximum TL intensity than other varying concentrations. The synthesis chemical reaction is shown in the below equation.

$$(1-x)BaCl_2 + (NH_4)_2SO_4 \xrightarrow{xEuCl_2+H_2O} Ba_{1-x}SO_4 : Eu_x + 2NH_4Cl$$

Where, $x = 0.3,\ 0.5,\ 1,\ 1.5,\ 2,\ 2.5\ and\ 3$ mol%.

3.2 Centrifuge

The centrifuge was used to separate the precipitate and salt mixture while synthesizing the Eu activated $BaSO_4$ material. The mixture contains the precipitates of $BaSO_4$ and NH_4Cl, which was kept in centrifuge revolved at 1000 rpm for 15 minutes. The process was repeated five times.

The centrifuge used was VWR Mega Star 600 (UK)[16] as shown in figure [3.2]. It is designed as an auto-lock rotator system. It features an aerosol-tight click-lock bucket cap and a rotator lid sealing system with time saving pulse capability with a clearly visible backlit display for easy parameter reading. There are two rotors, the TX-150 swing bucket rotor and the MicroClick 24×2 angle rotor. The first one is designed for a wide range of swing-out processes, providing high speed and high capacity for example $24 \times 5/7$ ml blood tubes or 8×15 ml conical tubes. The second rotor is a high-speed rotor with a maximum capacity of $24 \times 1.5/2.0$ ml micro tubes.

3.3 X-ray experiments

The x-ray experiments were performed in the Rontgen lab in the basement of the chemistry building, UiO. A PANTAK PMC 1000 X-ray unit was used for irradiation, which was operated at 100 kV, 160 kV, 225 kV, and 1 mA. Different filter combinations were used for specific X-ray potentials; 1.52 mm aluminum filter was used for 100 kV, 0.1mm copper and 2.02 mm aluminum were used for 160 kV, and 0.7 mm copper and 1.52 mm aluminum for 225 kV. X-irradiation were done on a Perspex plate at a source-to-detector distance of 50 cm.

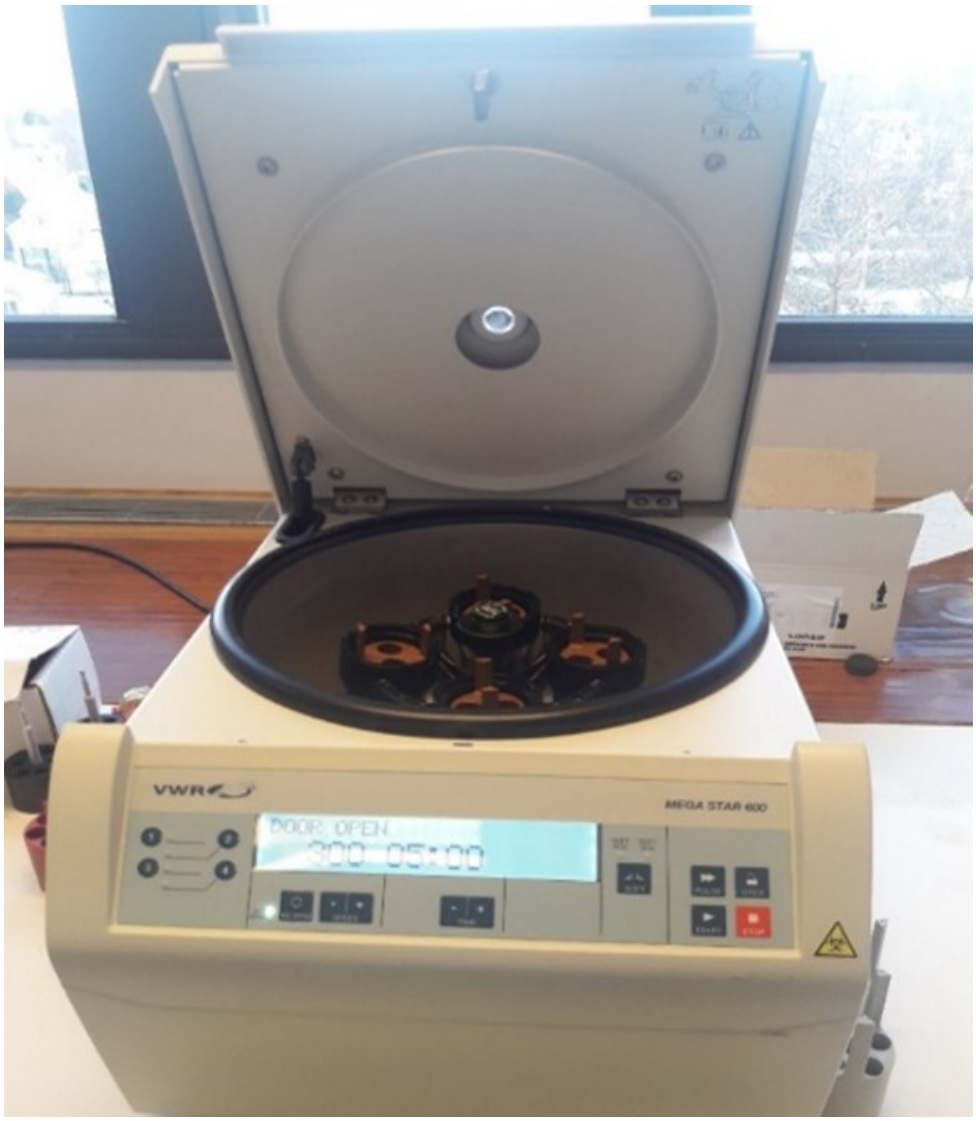

Figure 3.2. VWR Mega Star 600 centrifuge (UK).

During the calibration, a given tube potential was selected with proper filter combinations. Then the ionization chamber was joined with the electro-meter and was kept on the Perspex plate such that the sensitive volume of the ionization chamber lies at the center of the field as shown in figure [3.3].

Then, the X-ray tube was operated at the required potential with a 1 mA cathode current for 1 minute. The number of ionizations in the chamber appears as a charge on the electrometer in nC. The same experiment was repeated five times, showing that the electrometer reading was virtually constant. Thereafter, the value of D in the equation [3.3] was calculated. After this calibration, the dose rate on the Perspex plate was determined, from which time of irradiation for the required dose was calculated. The

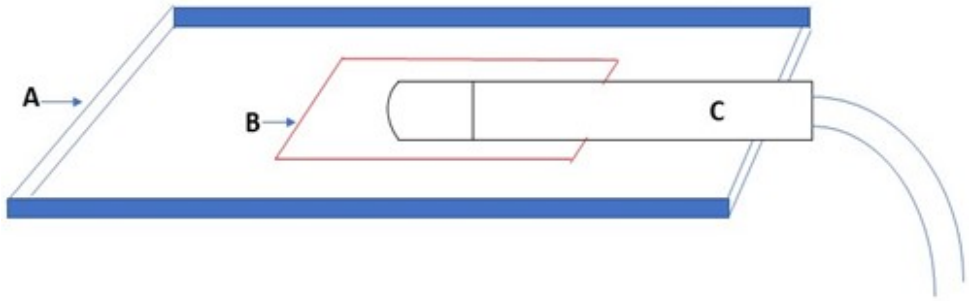

Figure 3.3. Schematic diagram of arrangement of ionization chamber on Perspex plate. A:Perspex plate, B:X-ray field, C:Ionization chamber.

whole experimental setup is shown in figure [3.4 left figure]. The ionization chamber has a plastic outer protective cover which ensures buildup of secondary radiation, but which also causes the sensitive volume to become elevated from the Perspex plate. For the samples to be irradiated at the same source-to-detector distance as the ionization chamber, they were placed on a 7.5 mm nylon6 plate. In addition, a 2 mm nylon6 plate placed on the top of the samples to ensure buildup of secondary radiation. The actual arrangement of the samples on the nylon6 plates as shown in figure [3.4 right figure].

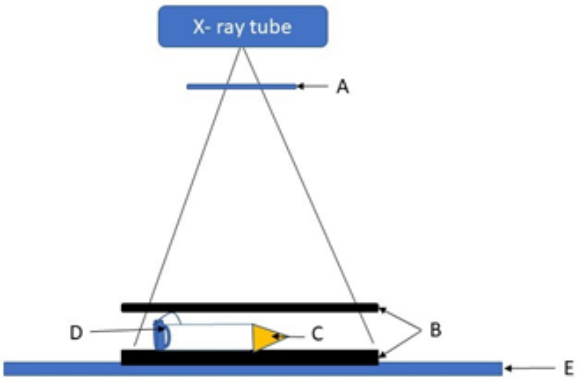

Figure 3.4. (Left) Schematic diagram of experimental setup for irradiation of sample; A: filters for X-ray, B: Nylon6 plates with thickness of upper plate 2mm and that of lower plate is 7.5 mm, C: Eu activated $BaSO_4$ sample, D: Microtube. E: Perspex plate at SSD of 50 cm. (Right); arrangement of samples on the nylon6 plate in the X-ray field on Perspex plate.

For X-ray experiments, 10 mg sample of europium doped barium sulphate was used. The X-rays of different voltages like 100, 160 and 225 kV were used with doses of 0.01, 0.02 and 0.03 Gy on nanocrystalline phosphor.

3.4 Co-60 source experiments

The experiments with γ-rays were performed in the Radium hospital with the Co-60 source (with mean quantum energy of gamma ray photons is 1.25 MeV) called Theratron T780C as shown in figure [3.5]. Prior to the irradiation, calibration was done by using an ionization chamber connected with an electrometer. The same ionization chamber and electrometer as for X-ray experiments was also used for Co-60 source experiments. The maximum field size of 42.6 $\times$ 42.6 cm was used for γ-rays. Now the dose deposited by γ-rays is given by

$$D = N_D M_u k_{TP} \tag{3.1}$$

Where N_D = 47.7 mGy/nC is the calibration factor due to absorbed dose to water, M_u is the electrometer reading and

$$k_{TP} = \frac{273.15 + T}{273.15 + T_0} \times \frac{P_0}{P} \tag{3.2}$$

k_{TP} is the correction for temperature and pressure. As like X-ray experiments, the calibration was done before the actual irradiation of the samples. The samples were placed on the top of a plastic plate and covered with another plate to obtain identical distance from the source as that of the sensitive part of ionization chamber.

Like X-irradiation, test irradiations for Co-60 γ-rays also lasted for 1 minute and were repeated it for 5 times. The resulting electrometer reading was very stable. The dose rate was thus calculated by using equation [3.1] and finally time for irradiation

Figure 3.5. Theratron T780C (Co-60 source device).

with specific doses could be calculated. The dose range was from 0.1 Gy to 1 Gy.

3.5 Ionization chamber and electrometer

The ionization chamber measures the dose deposited by ionizing radiation. When the gas-filled ionization chamber is placed in the ionizing radiation field, the radiation ionizes the gas and electrons are liberated; these electrons are detected by the electrometer connected across it. For our experimental work, IBA FC65-G ionization chamber (IBA Dosimetry, Germany)[17] was used as shown in figure [3.6].

The ionization chambers are sensitive to temperature and pressure, so during calibration, the estimated dose given by equation [3.3] contains a temperature and pressure correction factor . This type of chamber is intended for reference dosimetry and calibrations. The chamber can be used for electron beams and photons. It can also

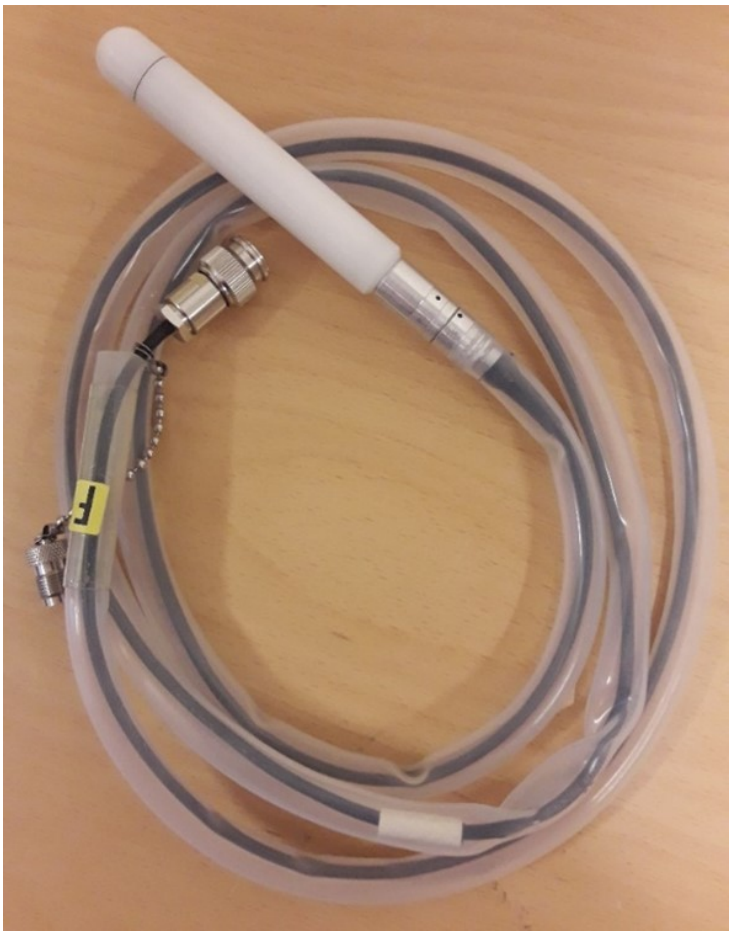

Figure 3.6. Theratron T780C (Co-60 source device).

be used for X-ray beams with operating potentials from 70 kV and for gamma radiation of Cs-137 and Co-60. The sensitive volume of it is 0.65 cm^3 with a total length of 23 mm. The operating polarizing voltage is $\pm$300 V with typical sensitivity of 21 nC/Gy. It can be operated in the temperature range of $15 - 35^{\circ}C$ and relative humidity of 20-80 %.

For the calibration, absorbed doses were measured by the above ionization chamber with a MAX-4000 electrometer (Standard Imaging, USA). The ion chamber was operated at 300 V. The irradiation time was set for 1 minute, and the amount of charge generated in the ionization chamber was recorded by the electrometer. The dose to water was determined according to IAEA report TRS 277 [18]

$$D = M_u N_k k_u (\frac{\bar{\mu}_{en}}{\rho}) p_u k_{TP} \tag{3.3}$$

Where M_u is the electrometer reading, N_k = (43.77± 0.39) mGy/nC is an air kerma calibration factor for the given quality, k_u = 1 is the correction factor for the change in response due to spectral distribution of the beam travelling from air to water, $(\frac{\bar{\mu}_{en}}{\rho})$ = 1.075 is the mass energy absorption co-efficient of water with relative to air, averaged over photon spectrum at reference depth, p_u = 1.02 is the perturbation correction factor, and k_{TP} is the correction factor for the temperature and pressure. This correction factor is given by

$$k_{TP} = \frac{273.15 + T}{273.15 + T_0} \times \frac{P_0}{P} \tag{3.4}$$

Where, $T_0 = 20°C$, T is the temperature in the X-ray chamber during measurement $(°C)$, $P_0 = 1013$ Pa, P is the atmospheric pressure at the time of measurement.

Electrometer

An electrometer is an instrument that is used to measure the amount of charge produced in the ionization chamber due to ionizing radiation. The electrometer supplies the required voltage to the ionization chamber. The MAX-4000 electrometer [19] used for calibration as shown in figure [3.7].

After the ionization chamber was joined with the electrometer, some general setting adjustments were done. The range of operation was selected at 'High' (indicating measurements in the nC-range) and dark current adjustment ('zeroing') was done by pressing start button. The electrometer takes around 10 minutes to stabilize.

This electrometer can measure currents in the range of 0.001 pA to 500 nA and charges range of 0.01 pC to 999999 nC. The leakage rate is very low less than 1 fA. Equipped with a digital filter that eliminates the effect of noise, achieving stable results

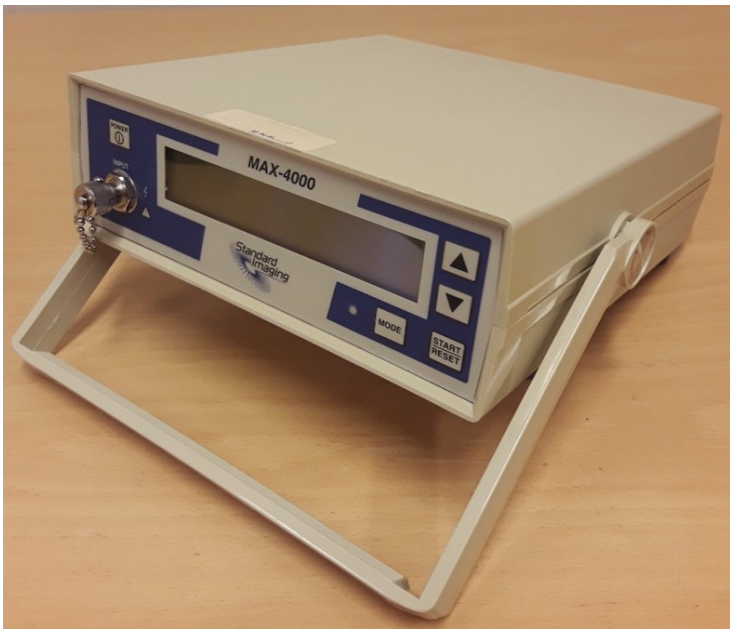

Figure 3.7. MAX-4000 electrometer (Standard Imaging, USA).

and highly accurate measurements.

3.6 TLD reader

The signals present in the sample after irradiation was analyzed with the help of an instrument called a RedPro TLD reader. We used a TLD Cube (RedPro Frieberg Instruments, Germany) [20], as shown in the figure [3.8]. It is a small portable TLD reader used for measuring, analyzing, and evaluating the thermoluminescent material. It consists of ceramic heating and pressurized air as a cooler.

The reader is mainly divided into three parts as heating system, light detector, and output recorder. The TLD cube has a single element reader with a TL measurement chamber. It can heat the sample to 600°C (endpoint temperature) and has a photo-sensor that can detect the light range of 300-650 nm wavelength. The 'TL Studio' is used as an operating and evaluating software by which live data visualization can be done. The software is professionally designed for data acquisition, storage, and export. This device has an accuracy of 1 % of standard deviation for multiple readouts. Four

different heating rates can be adjusted starting from 5, 10, 15, and 20 K/s.

The thermoluminescent material in the shape of typically a powder was placed on the sample holder and inserted into the TLD reader. The heating rate and endpoint temperature were set by using software installed in the computer connected to the TLD reader. The thermoluminescence was recorded by the photo multiplier tube in the reader.

Figure 3.8. RedPro TLD reader (Frieberg Instruments, Germany)[20].

The software called 'TL Studio' records the intensity of light emitted as the function of the corresponding temperature and plots the live curve between them. The output obtained can be saved in Excel, comma-separated values (CSV) and extensible markup language (XML) format.

3.7 Annealing Furnace

Annealing is the phenomenon of removing the residual signals present in thermoluminescent material by heating at high temperature for certain duration. The annealing of TLD material is carried out after the output is taken from it. The dosimetric materials can be reused, if we use them without annealing, the residuals may affect the sensitivity of the material. For annealing the TL material, a Nabertherm sintering furnace (Germany)[21] with lift door model was used which is shown in the figure [3.9].

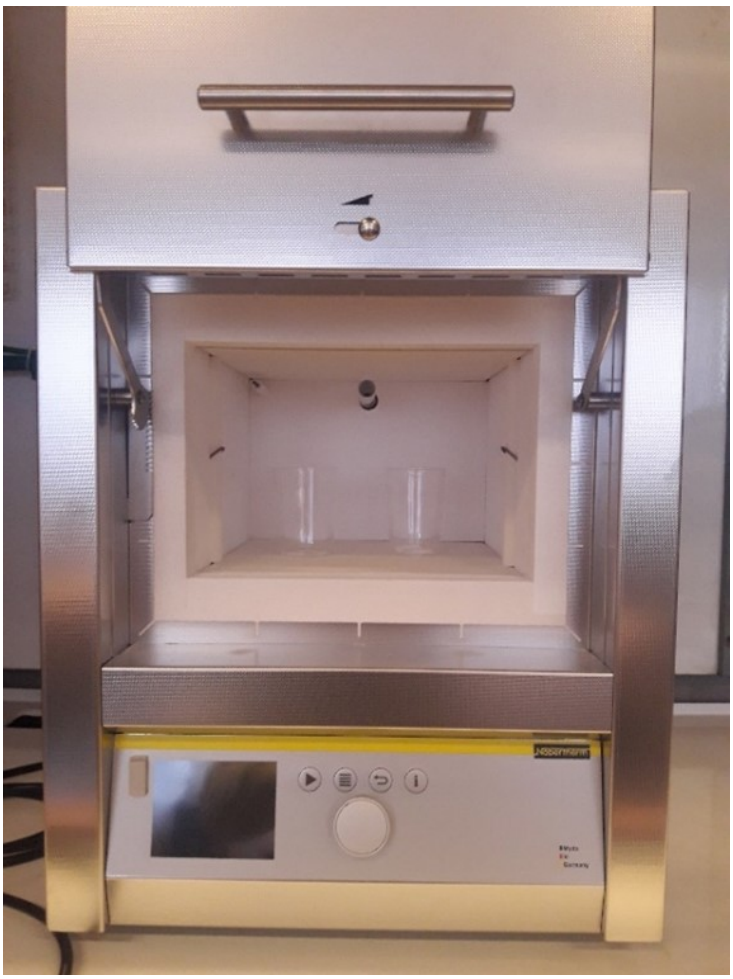

Figure 3.9. Nabertherm sintering furnace Oven (LT-9/11, Germany).

For annealing, the TL material was placed in a quartz glass furnace and was placed in the oven by setting the temperature of 400°C for 30 minutes.

It is standard equipment in the laboratories for daily use. This oven is known for excellent quality, advanced design, and is highly reliable. It has two-sided heating

ceramic plates for maximum temperature uniformity and an operating temperature of $1100^{\circ}C$ (Maximum temperature). There is a hot surface lift door facing the other side of the operator, with a hot air outlet from the back wall of the oven. There are controllers for various heating programs. The oven has a double stainless-steel casing with an additional fan for cooling.

3.8 EPR dosimeter

For EPR dosimetry, the samples of Eu activated $BaSO_4$ was irradiated with X-rays with tube potential of 225 kV with cathode current of 10 mA at SSD of 50 cm. The samples were irradiated with 1 Gy, 2 Gy and 3 Gy. These samples were stored for 24 hours in a dark place. The EPR experiments were performed to see if these samples gave an EPR signal that would indicate a potential for EPR dosimetry. We used an EleX-syS560 Super X EPR/ENDOR spectrometer, as shown in figure [3.10].

Figure 3.10. EleX-syS560 Super X EPR/ENDOR Spectrometer.

Several resonances from irradiated samples were observed at different frequencies. The peak-to-peak value around the main resonances of EPR spectrum was extracted and a curve was plotted to see the relation between dose and EPR level.

Chapter 4

Experimental Results

Science proceeds more by what it has learned to ignore than what it takes into account.

-GALILEO GALILEI

4.1 Irradiation with Co-60 source

10 mg of Eu activated barium sulphate phosphor sample was irradiated with radiations. The dose range for irradiation was from 0.1 Gy to 1 Gy. For each dose four samples were used.

The ion chamber calibration was done before the irradiation of the TL material; for each dose, the time of irradiation was calculated. From the calibration, the irradiation time for 0.1 Gy was found to be 26 seconds. Similarly, for 0.2 Gy, the irradiation time is 26×2 s, and for 0.3 Gy is 26×3 s and so on up to 1 Gy. The irradiated sample is then stored in the dark at room temperature for 24 hours, and the TL measurement was then done using the TLD cube. The data thus obtained are plotted as temperature versus TL

intensity curve. As we have used four samples for each dose, presented glow curves in figure [4.1] are the average for each dose.

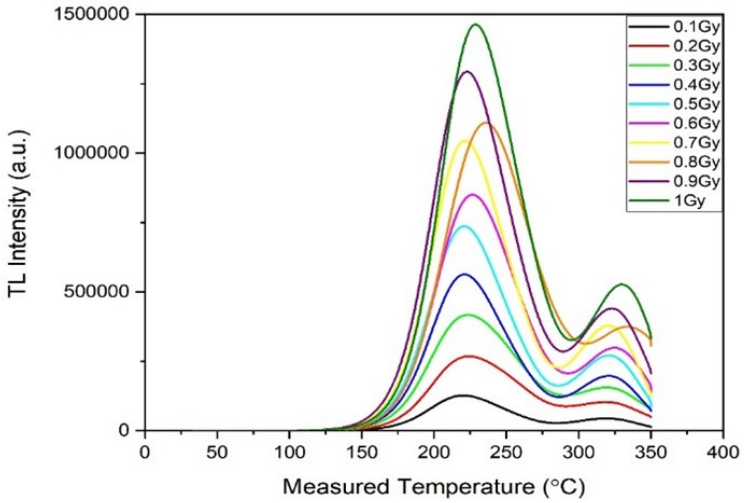

Figure 4.1. Glow curves, i.e., temperature °C vs TL intensity plots, where each curve is for different doses as indicated by the colors.

In figure [4.1], we see that the TL intensity is proportional to the dose. To further quantify the dose response relationship, the peak intensity for each sample was plotted against dose together with a linear regression on the data [4.2].

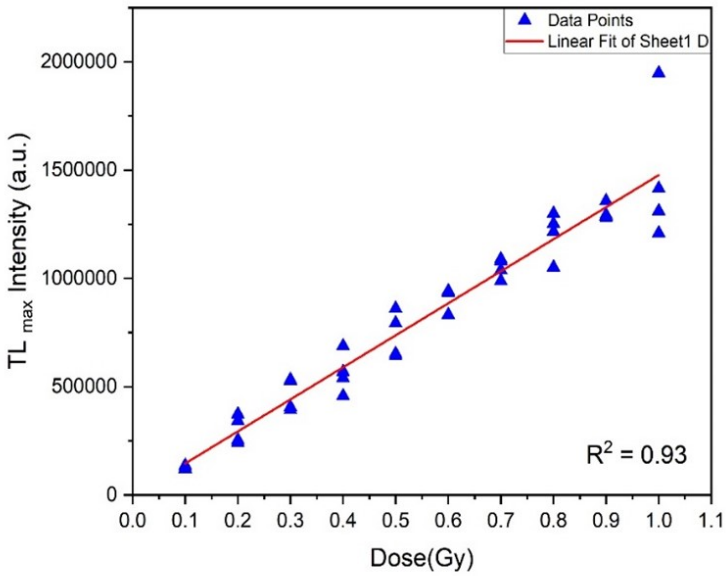

Figure 4.2. TL peak intensity vs dose including linear regression for Co-60 irradiation. The goodness-of-fit (R^2 value) is given.

The maximum intensity obtained for each sample was plotted against the dose, and the regression line with a linear regression coefficient. The graph confirms the proportionality of TL intensity with dose.

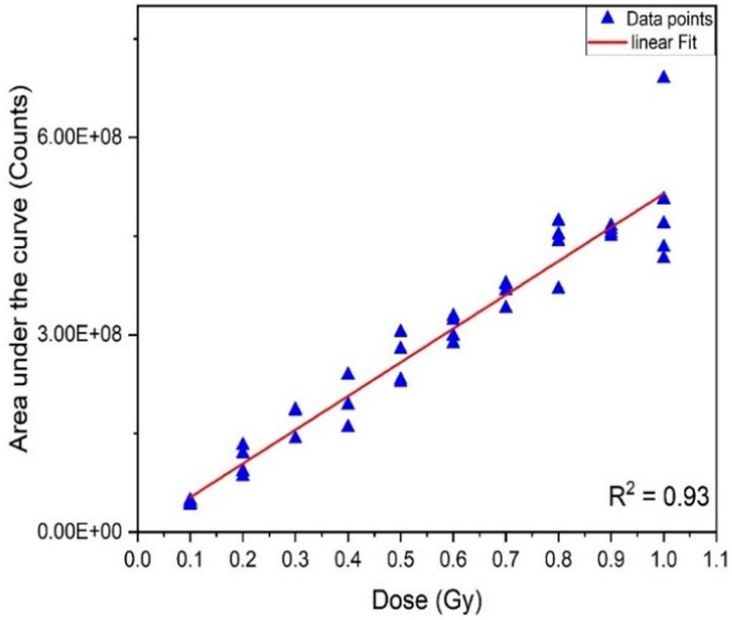

Figure 4.3. TL area under glow curve vs dose including linear regression for Co-60 irradiation. The goodness-of-fit (R^2 value) is given.

As explained in chapter 3, different dose-related metrics can be derived from the TL glow curves, and the area under curve is an alternative to peak intensity. In figure [4.3] the area under the glow curve is plotted against the dose. Here, a goodness-of-fit of $R^2 = 0.93$ was obtained, which is identical to that for peak intensity.

4.2 Irradiation with X-rays

X-rays are produced by striking the fast-moving electron beam with a heavy metal target. The X-rays thus produced are the spectrum consisting of energy ranging from a minimum to a maximum. The spectrum of consists of characteristics X-rays as well as bremsstrahlung. The sharp peaks in the X-ray spectrum (as shown in figure [4.4]) are the characteristic X-rays, and the smooth part in the spectrum are the X-rays due to

bremsstrahlung.

We used X-rays of energy 100 kV, 160 kV, and 225 kV for this project work with different filter arrangements. The program called "SpekCalc" was used to find the X-ray spectrum of different energies with varying combinations of the filter. For example, the X-ray spectrum at 100 kV using a 1.52 mm Aluminum filter is shown in figure [4.4]. The mean energy of this spectrum with filter 1.52 Al was found to be 45.17 keV. Similarly, the X-ray spectrum of 160 kV with filter 0.1 mm Cu and 2.02 mm Al was also calculated with the same program, and the mean energy was found to be 67.089 keV. Moreover, the spectrum of 225 kV X-rays with filter 0.7 mm Cu and 1.52 mm Al, the mean energy was found to be 97.46 keV.

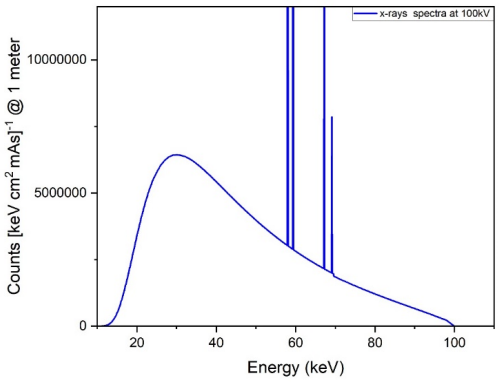

(a) Image a

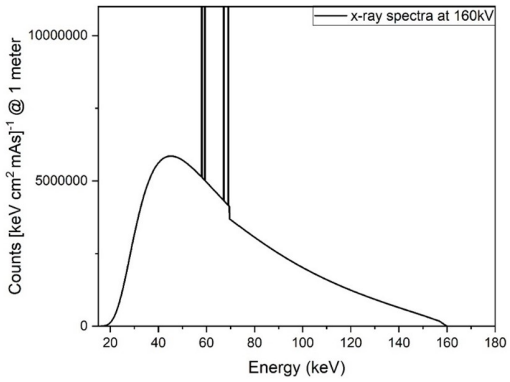

(b) Image b

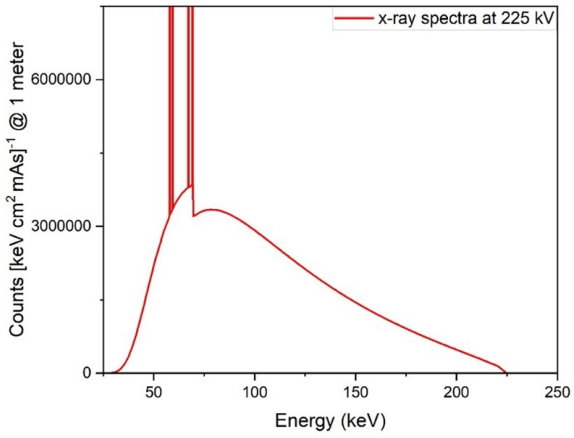

(c) Image c

Figure 4.4. X-ray spectrum at Image a.) 100 kV using 1.52 mm Al filter, Image b.) at 160 kV using 0.1 mm Cu and 2.02 mm Al filter and Image c.) at 225 kV using 0.7 mm Cu and 1.52 mm Al filter

I. Irradiation with 100 kV X-rays

The thermoluminescence property of Eu activated $BaSO_4$ is also tested by irradiating the sample of phosphor with X-rays. The X-ray facility is available at Roentgen lab in the basement of chemistry building. 10 mg sample of Eu activated $BaSO_4$ is irradiated at different energies like 100 kV, 160 kV and 225 kV and the results obtained are described in detail below.

The ion chamber calibration was done before the actual TL sample irradiation. For 100 kV X-rays, 1.52 mm of Al filter was used with source-to-detector of 50 cm. The filament current was 1 mA, and the dose received by the chamber at SD was calculated by using the ionization chamber placed at SD. The dose range for 100 kV X-ray irradiation was from 0.01 Gy to 0.03 Gy. For each dose, three samples of 10mg phosphor were irradiated. Then TL measurement of the samples were done in the TLD cube reader. The peak intensity versus dose, together with a linear regression curve, is shown in figure [4.5]. In this figure, we see that the TL maximum intensity approximately increases linearly with dose. The goodness-of-fit from the regression was $R^2 = 0.96$, which confirms a high degree of linearity.

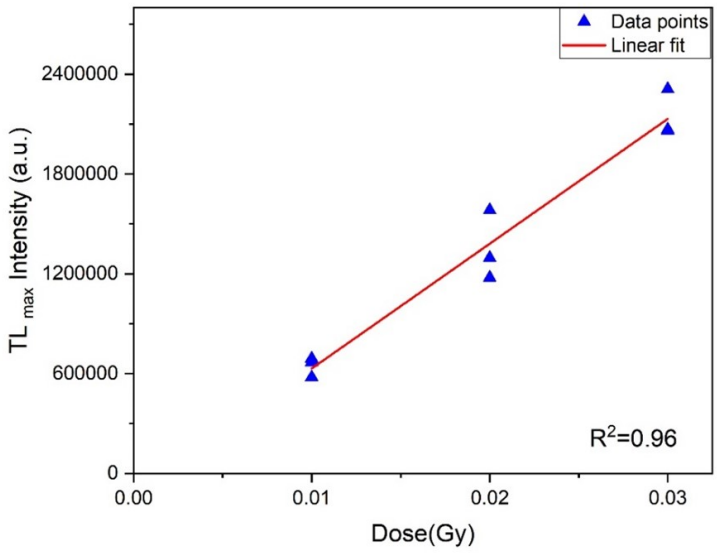

Figure 4.5. TL peak intensity vs dose including linear regression for X-rays. The goodness-of-fit (R^2 value) is given.

II. Irradiation with 225 kV X-rays

For 225 kV energy, 1.52 mm Al and 0.7 mm Cu filter was used. The phosphor was irradiated with dose range starting from 0.01 Gy to 0.03 Gy. After irradiation the output of the sample was analyzed in a TLD reader. The peak intensity versus dose together with linear regression curve is plotted as shown in figure [4.6].

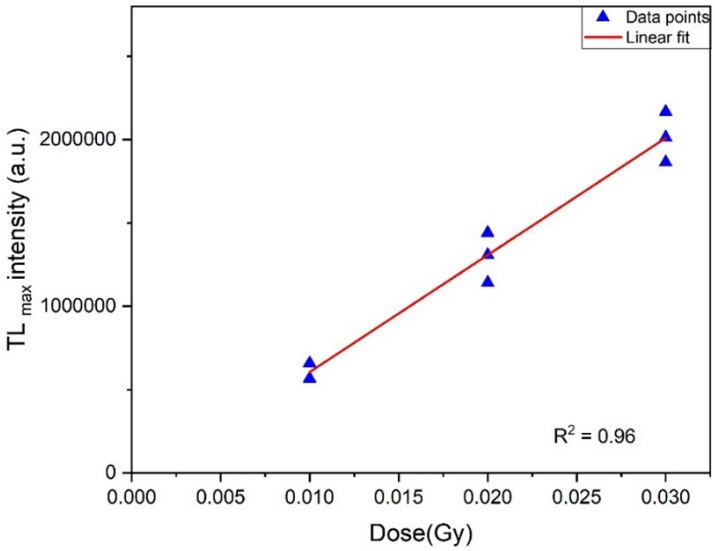

Figure 4.6. TL peak intensity vs dose including linear regression for X-rays. The goodness-of-fit (R^2 value) is given.

Also in the same figure, we see that the TL maximum intensity approximately linearly increases with dose. The linear correlation coefficient with $R^2 = 0.96$, confirms the high degree of linearity.

4.3 Comparison between 100 kV and 225 kV X-rays

Here, we compare the results obtained above for 100 kV and 225 kV X-rays as shown in figure [4.7]. The slopes for 100 and 225 kV lines are $(7.5 \pm 0.57) \times 10^7$ and $(7.02 \pm 0.57) \times 10^7$, respectively, indicating the sensitivity of the material to the given

radiation quality. From the plot, it was found that the slope at 100 kV ≈ slope at 225 kV. Therefore, the sensitivity of $BaSO_4$ is almost similar at 100 kV and 225 kV. Also, the details on the irradiation of $BaSO_4 : Eu$ with X-ray can be found in section Appendix [A].

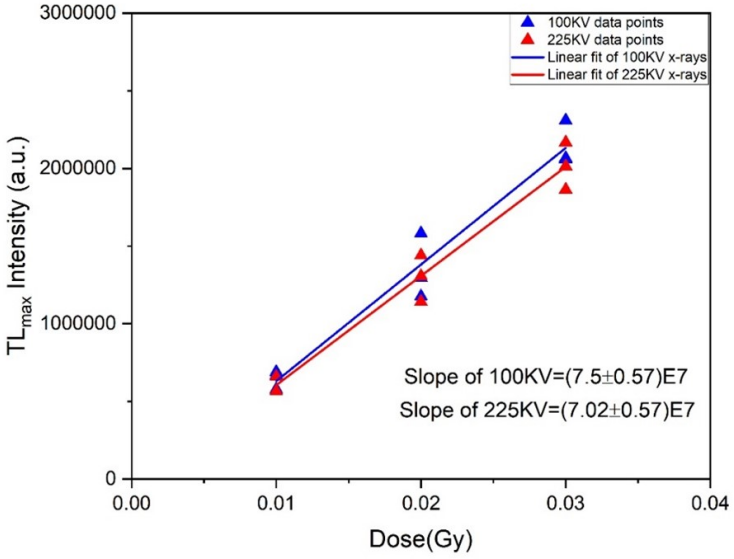

Figure 4.7. TL max intensity versus dose for 100 kV and 225 kV plotted together including slopes of the regression lines.

4.4 Comparison between 100 kV, 225 kV X-ray and Co-60 source

When X-rays and γ-rays interact with matter, there are different types of interaction phenomena that takes place like photoelectric effect, Compton effect, and pair production. The type of interaction that is dominant depends upon both the energy of photon as well as the atomic number of the matter, which can be clearly seen in the figure [2.1]. In dosimetry, we are primarily interested in the dose to water, as the human tissue and water have almost the same atomic number and radiation dose deposition will be very similar.

The effective atomic number ($BaSO_4$ and water are compounds) of water is 7.42,

and $BaSO_4$ is 46.9, respectively. Thus, the effective atomic number of $BaSO_4$ is much larger than water so the energy deposition in the two compounds will be different. The energy deposition from photons in a matter is proportional to mass energy absorption co-efficient $(\frac{\mu_{en}}{\rho})_{E,Z}$.

The absorbed dose is given by

$$D = \Psi \left(\frac{\mu_{en}}{\rho} \right)_{E,Z} \tag{4.1}$$

Now, the mass energy co-efficient of $BaSO_4$ can be calculated by using Bragg's law. Therefore,

$$\left(\frac{\mu_{en}}{\rho} \right)_{BaSO_4} = \left(\frac{\mu_{en}}{\rho} \right)_{Ba} f_{Ba} + \left(\frac{\mu_{en}}{\rho} \right)_{s} f_s + \left(\frac{\mu_{en}}{\rho} \right)_{o_2} f_{o_2} \tag{4.2}$$

Where f_{Ba}, f_s, f_{o_2} and are the weight fractions of corresponding materials and are given by f_{Ba}=0.58799, f_s= 0.13739, and f_{o_2}= 0.2742. The mass-energy absorption coefficients may be found at NISTs web pages for given materials and energies [22].

For γ-radiations, the average energy of photon beam is around 1.25 MeV so, the mass energy absorption co-efficient for Ba, S and O_2 is taken at that energy. Thus, $\left(\frac{\mu_{en}}{\rho} \right)_{Ba} = 2.388 \times 10^{-2}$, $\left(\frac{\mu_{en}}{\rho} \right)_{s} = 2.65 \times 10^{-2}, and \left(\frac{\mu_{en}}{\rho} \right)_{o_2} f_{o_2} = 2.67 \times 10^{-2}$.

By putting all these values in the equation [4.1], we have $\left(\frac{\mu_{en}}{\rho} \right)_{BaSO_4} = 2.48 \times 10^{-2}$ for $\gamma - rays$.

Similarly, for X-rays of energy 225 kV, we can calculate mass absorption co-efficient for $BaSO_4$. Therefore, $\left(\frac{\mu_{en}}{\rho}\right)_{BaSO_4} = 8.67 \times 10^{-1}$ (for x-rays of 225 kV).

Also, the mass energy co-efficient for water is given by $\left(\frac{\mu_{en}}{\rho}\right)_{H_2O} = 2.97 \times 10^{-2}$ (for γ-rays) and $\left(\frac{\mu_{en}}{\rho}\right)_{H_2O} = 2.55 \times 10^{-2}$ (for X-rays of 225 kV).

Now from equation [4.1], the dose deposited in $BaSO_4$ by the γ-rays are given by

$$D_{BaSO_4} = D_W \left[\frac{\left(\frac{\mu_{en}}{\rho}\right)_{BaSO_4}}{\left(\frac{\mu_{en}}{\rho}\right)_{H_2O}}\right] = D_W \times 8.35 \times 10^{-1} \tag{4.3}$$

And the dose deposited in $BaSO_4$ by X-rays are

$$D_{BaSO_4} = D_W \times 3.41 \times 10^{-1} \tag{4.4}$$

Solving equations [4.3] and [4.4] we have,

$$(D_{BaSO_4})_{x-ray} = 41 \times (D_{BaSO_4})_{\gamma-ray} \tag{4.5}$$

Hence, from theoretical calculations, it is found that $BaSO_4$ is 41 times more

sensitive to x-rays of energy 225 kV than that of γ-rays having energy 1.25 MeV.

Again, the mean energy of 100 kV beam is around 50 keV, the mass absorption coefficient for $BaSO_4$ is $\left(\frac{\mu_{en}}{\rho}\right)_{BaSO_4} = 3.91$ and that of water is $\left(\frac{\mu_{en}}{\rho}\right)_{H_2O} = 4.22 \times 10^{-2}$. By comparing these values with equation [4.3], $(D_{BaSO_4})_{x-ray} = 111 \times (D_{BaSO_4})_{\gamma-ray}$. So, $BaSO_4$ is 111 times more sensitive to X-rays of energy 100 kV than that of γ-rays having energy 1.25 MeV. To justify the theoretical calculation with the experimental results, the data obtained from the irradiation of 10 mg sample of $BaSO_4$ with X-rays of energies 100 kV and 225 kV and that of Co-60 γ-rays were plotted in a single graph to compare the sensitivity of the material with different radiations and energies. The linear regression curves for X-rays (100 kV and 225 kV) and Co-6o γ-rays are shown in figure [4.8].

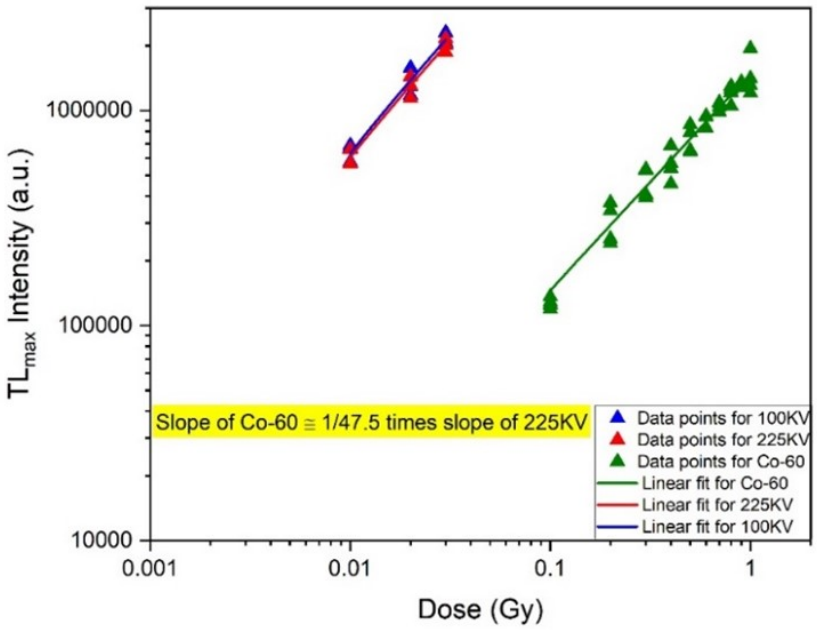

Figure 4.8. TL_{max} intensity versus dose for 100 kV and 225 kV for X-rays and Co-6o γ-rays plotted together with compared slopes of 225 kV X-rays and γ-rays.

The slope of linear regression curve (TL reading vs dose) gives the dose sensitivity. The slope for 225 kV X-rays are $(7.02 \pm 0.57) \times 10^7$ and that for Co-60 γ-ray is $(1.48 \pm 0.62) \times 10^6$ respectively. If we compare the slopes of these two lines, the dose sensitivity of the X-rays was found to be nearly equals to 47.5 times the dose sensitivity

of γ-rays, which is quite close to our theoretical value of 41.

As the sensitivity of 100 and 225 kV X-rays was almost similar, so we want to find an energy that has even higher sensitivity than these two energies. We use the program "SpekCalc" to find the energy with a suitable filter to obtain approximately maximum X-ray sensitivity. That energy was found to be 160 kV with 0.1 mm Cu and 2.02 mm Al filters.

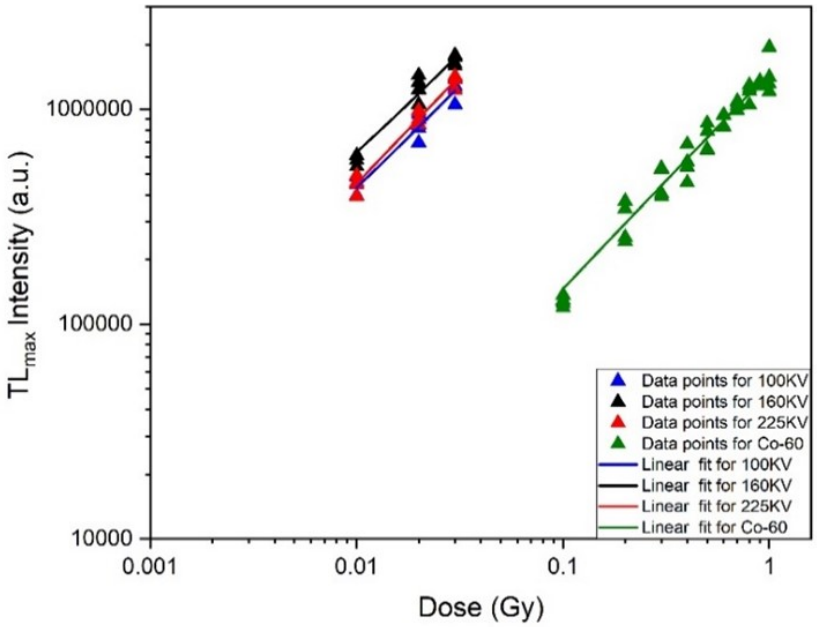

Figure 4.9. TL_{max} intensity versus dose for 100 kV, 160 kV and 225 kV for X-rays and Co-6o γ-rays plotted together.

Now a new set of samples of 10 mg Eu activated $BaSO_4$ were irradiated with X-ray voltages of 100 kV (with filter1.52 mm Al), 160 kV (with filter 0.1 mm Cu and 2.02 mm Al), and 225 kV (with filter 1.52 Al and 0.7 mm Cu). The output of TL reading was plotted as a function of dose together with linear regressions and compared with Co-60 γ-rays as shown in figure [4.9].

Now, from this plot, it was found that the sensitivities of $BaSO_4$ were to less than the previous experiment with the same energies 100 and 225 kV by using the same filters and same SSD (further elaborated in the Discussion chapter). Thus, to compare

findings to the reference experiments, where also Co-60 irradiation were done, there is a need for a correction of the slopes of the linear regression curve of different energies between experiment 1 and experiment 2. This process is outlined below.

Correction factor for sensitivity (slopes) of experiments 1 and 2

For experiment 1

Slope of linear regression curve for 100 kV X-rays = 7.50×10^7
Slope of linear regression curve for 225 kV X-rays = 7.02×10^7

For experiment 2

Slope of linear regression curve for 100 kV X-rays = 3.94×10^7
Slope of linear regression curve for 225 kV X-rays = 4.54×10^7
Slope of linear regression curve for 160 kV X-rays = 5.5×10^7

The correction factor is given by

$$C_{12} = \frac{1}{2}\left(\frac{s_{(225)1}}{s_{(225)2}} + \frac{s_{(100)1}}{s_{(100)2}}\right) = \frac{1}{2}\left(\frac{7.02 \times 10^7}{4.54 \times 10^7} + \frac{7.50 \times 10^7}{3.94 \times 10^7}\right) = 1.47.$$

Now, new slope of linear regression curve for 100 kV X-rays = $(3.9 + 1.47) \times 10^7 = 5.37 \times 10^7$
Also slope of linear regression curve for 160 kV X-ryas = $(5.5 + 1.47) \times 10^7 = 6.97 \times 10^7$
And slope of linear regression curve for 225 kV X-rays = $(4.5 + 1.47) \times 10^7 = 5.97 \times 10^7$

The data from experiment 1 and 2 for 100 and 225 kV gives slopes of 1/2(7.5+6.7) = 7.1 and 1/2(7.74+7.0) = 7.3 respectively. Relative to Co-60 slope for experiment 1 (=

0.15), we now have the sensitivity ratios **47, 49,** and **63** for 100 kV, 225 kV and 160 kV.

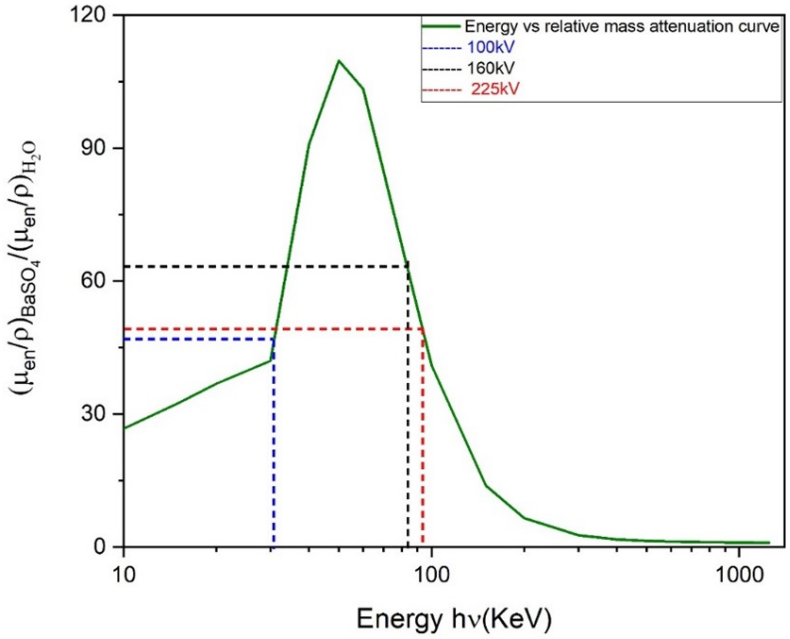

Figure 4.10. Plot between monoenergetic photon energy (keV) and relative mass attenuation coefficient of $BaSO_4$ normalized to photon energy 1.25 MeV [22].

The slopes of linear regression curves for X-ray potentials 100, 160, and 225 kV after the correction were compared with the Co-60 irradiation. Now a plot between monoenergetic photon energy and the ratio of mass attenuation of $BaSO_4$ and water was plotted as shown by the green curve in figure [4.10]. The corrected slopes of X-ray energies are now plotted as a sensitivity compared to the Co-60 source normalized to the energy of 1.25MeV.

The sensitivity of monoenergetic photons at 1.25 MeV was compared with the sensitivities of 100, 160, and 225 kV spectra; the sensitivities were found to be 47, 49 and 63 respectively. The sensitivity for 225 kV is almost like the theoretical value of 41 in equation [4.5]. These sensitivities are now indicated as vertical-horizontal lines in figure [4.10]. The blue 'dashed' line represents sensitivity corresponding to 100 kV, black for 160 kV and red for 225 kV respectively. From these lines, we can find a representative 'effective' monoenergetic X-ray energy for the given experimental X-ray spectrum. From Figure [4.10], we find that the effective energies for 100 kV, 160 kV and 225 kV are 19 keV, 94 keV, and 100 keV respectively.

4.5 Heating rate effect

The TLD material $BaSO_4$ also shows a heating rate effect. 10 mg sample of Eu activated $BaSO_4$ phosphor was irradiated with 225 kV X-rays with dose of 0.01 Gy. The dosimeter signal was read by the TLD cube system. Four different heating rates were used such as 5, 10, 15, and 20 K/s. The output of the TLD reader was then plotted as a function of temperature versus TL intensity, which is shown in figure [4.11]. The glow curve thus plotted is the mean of all sets of sample (minimum four samples) output.

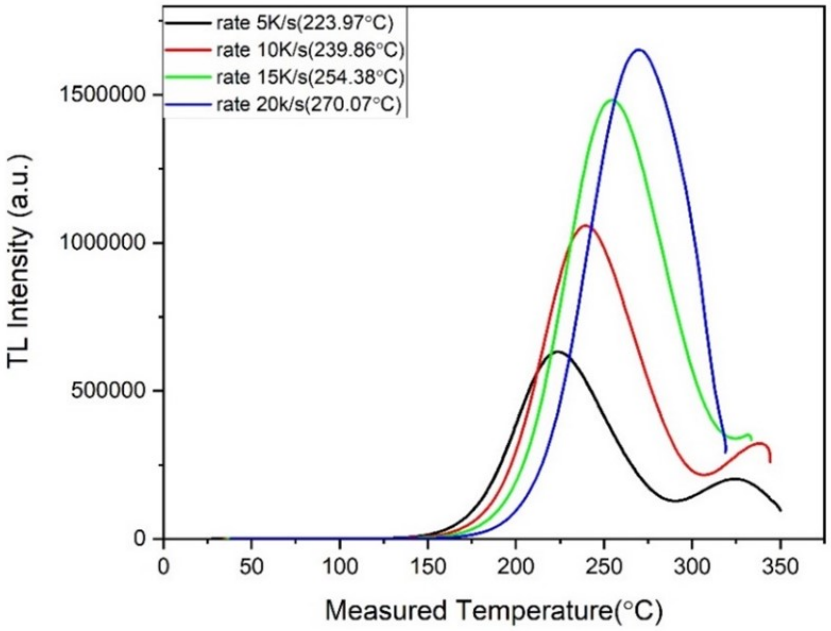

Figure 4.11. Glow curve between applied temperature (°C) and TL intensity (a.u.) with four different heating rates starting from 5 K/s to 20 K /s.

In the glow curve spectra, the heating rate of 5, 10, 15 and 20 K/s is represented by a black, red, green, and blue curve respectively. The peak value of TLmax intensity at the different heating rates was found at temperatures $224°C$, $240°C$, $254°C$, and $270°C$ respectively. From the spectra, the faster heating rates produce a shift in temperature toward higher values of TL_{max}. The TL maximum intensity was plotted against heating rate together with an applied linear regression in figure [4.12]. The value of $R^2 = 0.95$ suggests a high goodness of fit that it is evident that TL intensity increases linearly

with the heating rate.

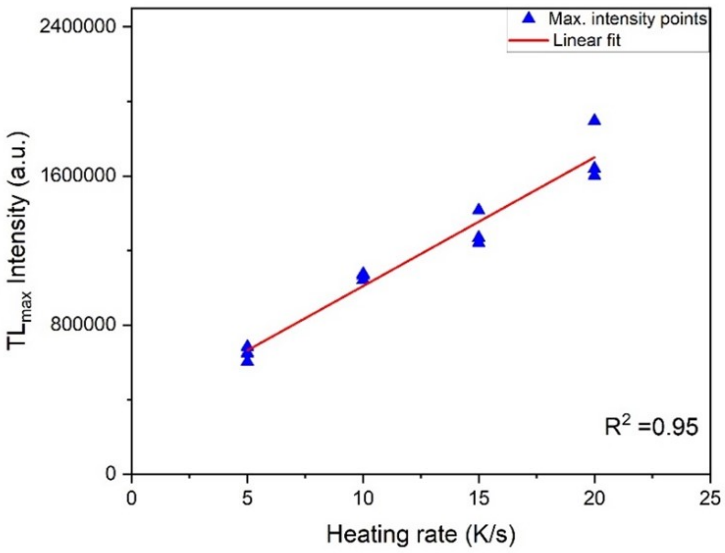

Figure 4.12. TL_{max} intensity as a function of applied heating rates. A linear regression curve with corresponding goodness of fit (R^2 value) is also given.

In the plot between heating rate and area under the curve, it was observed that as the heating rate increases, the area under the curve decreases, although TL_{max} intensity increases towards the high-temperature side, figure [4.13 Plot-A].

That means the glow peak becomes narrower with the increasing heating rate, thereby increasing the TL intensity, but the area under the curve decreases, which leads to suspects about the TL residuals in the sample. Therefore, a separate experiment was performed to test the TL residuals present in the sample after different heating rates. To check the residuals, the samples that were used for heating rate analysis are again heated by a constant heating rate of 5 K/s. The signals obtained from these are now plotted area under the curve as a function of heating rate. The mean of individual data was plotted as shown in figure [4.13 Plot-B]. From the experiment of residual analysis, it was observed that the TL residual signals present in the sample increases with heating rate.

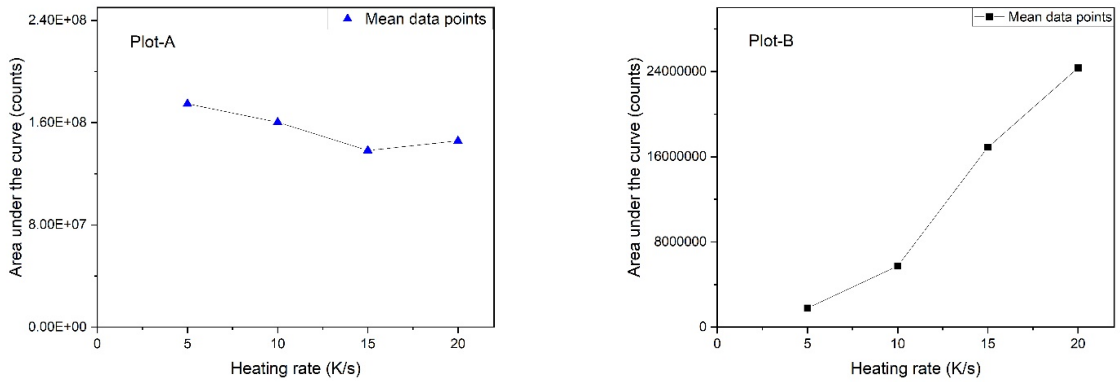

(a) *(b)*

Figure 4.13. Plot-A: Area under the glow curve as a function of heating rate for initial experiment. Plot-B: Area under the glow curve as a function of heating rate for residual signals.

4.6 Reusability Test

The reusability of a dosimeter material is an essential property of it. The dosimeter material can be reused if it does not lose its properties after the removal of TL residual signals from it by the process of annealing.

To test the reusability of Eu activated $BaSO_4$, four samples of 10 mg of it were irradiated by 225 kV X-rays, and they were stored in the dark for 24 hours. Now, these samples were heated at the rate of 5 K/s using the TLD cube reader, and the output was noted. The annealing of the samples was done (after TLD reading) at $400^{\circ}C$ for 30 minutes. Again, the samples were irradiated for another cycle, and the same phenomenon of irradiation followed by TLD measurement and finally annealing is repeated for ten consecutive cycles. The output of TLD measurement is now plotted as a glow curve between temperature and TL intensity, as shown in figure [4.14].

In the figure, it can be clearly noted that the glow curve for cycle 1 has significantly higher intensity as compared to other cycles, and after the first cycle, the intensities of all other cycles are comparable. Also, in cycle 6, the glow curve has the lowest intensity, and the curve does not contain a second peak. A graph was plotted between the number of cycles and mean area (minimum four samples) under the curve is shown

in figure [4.15]. It can be clearly seen that the TL intensity decreases after the first cycle and remains almost constant for the rest of the cycles.

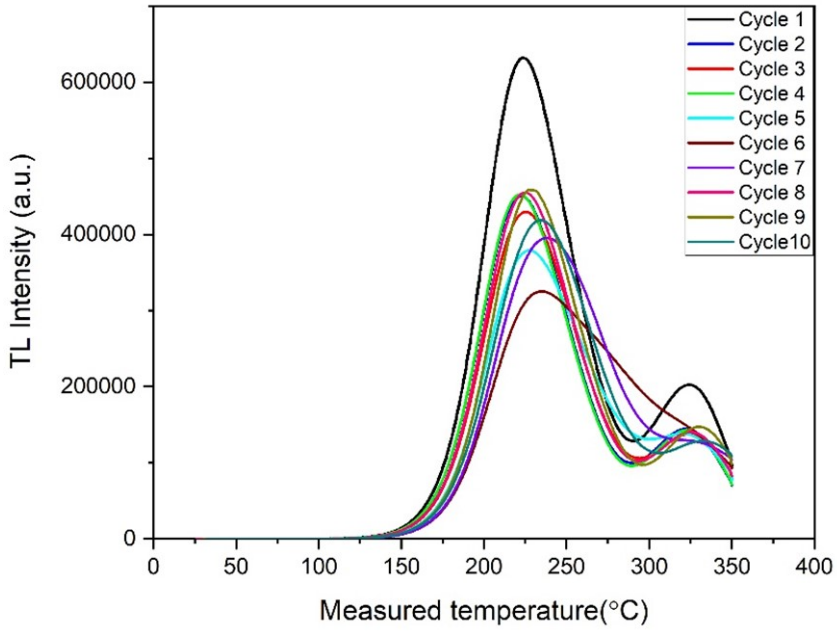

Figure 4.14. Glow curve between temperature (°C) and TL intensity (a.u.) for reusability test of up to 10 cycles.

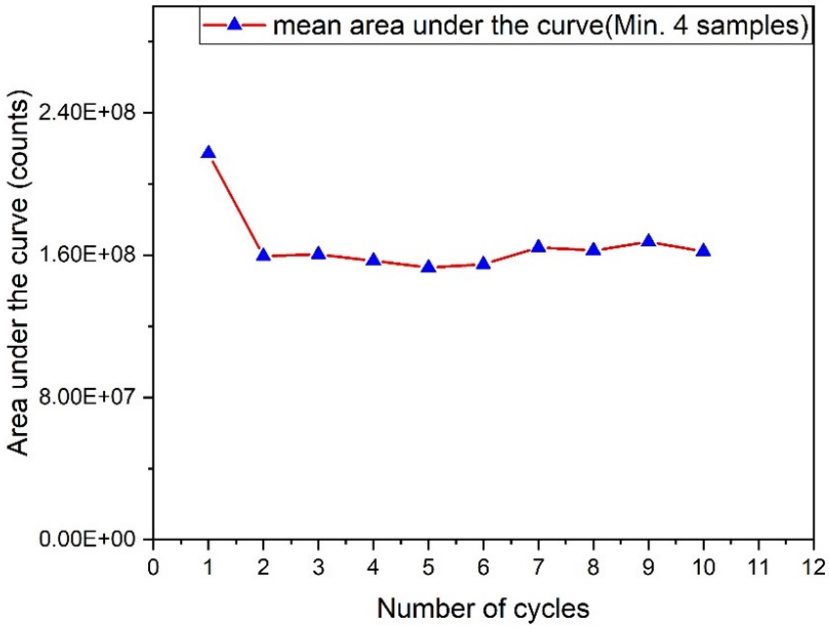

Figure 4.15. Plot between number of cycles and area under the curve.

The reusability of the TL response of nanocrystalline barium sulfate doped with

europium for dosimetric purpose can be determined by a parameter called reproducibility parameter which is given by equation [23].

$$R = \frac{100\sigma}{\bar{x}} \leq 7.5\% \tag{4.6}$$

Where, σ is the standard deviation and $\bar{x}$ is the average of all the reading taken during the ten cycles. On calculating the reproducibility or reusability for ten cycles was found to be 1.20 and that for last nine cycles excluding the first cycle was found to be 0.336. Which is well below 7.5%. The observed values of reproducibility parameter are with in the acceptable value.

4.7 Fading

The dosimeter material must have stable traps to store the signals without having any loss of signal or fading. 10 mg samples of Eu activated $BaSO_4$ were irradiated by a Co-60 source with a dose of 0.5 Gy and were placed in the dark to avoid any unnecessary signal loss from exposure to sunlight. Five days after the irradiation, the output signals of 3 samples were noted by using the TLD cube. Now, for the next cycle, the gap between consecutive cycles was five days, and the process continued for 50 days for ten cycles. The output obtained from the TLD reader was plotted as a glow curve between temperature and TL intensity, as shown in figure [4.16]. The glow curve from day 5 to day 50 is denoted by different colored lines.

From the glow curves we cannot observe much decrease in the TL intensity at the end of 50 days but on the 35^{th} day there is a drop in intensity. To figure out what the expected loss of signal at the end of 50 days, a linear regression was plotted together with TL maximum intensity vs time curve in figure [4.17]. As seen, there is small

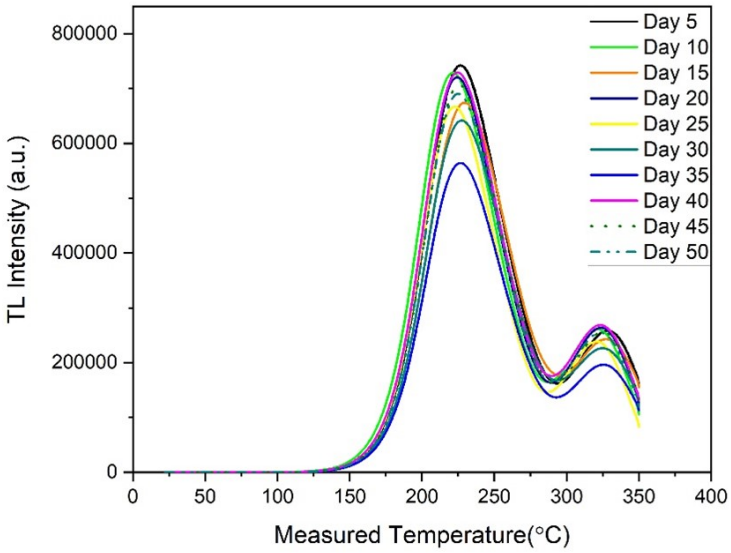

Figure 4.16. TL intensity vs temperature for samples measured at different times after irradiation.

decrease in intensity up to 50 days. The relative slope of the linear regression curve is negative. Now, fading can be calculated by using a relation

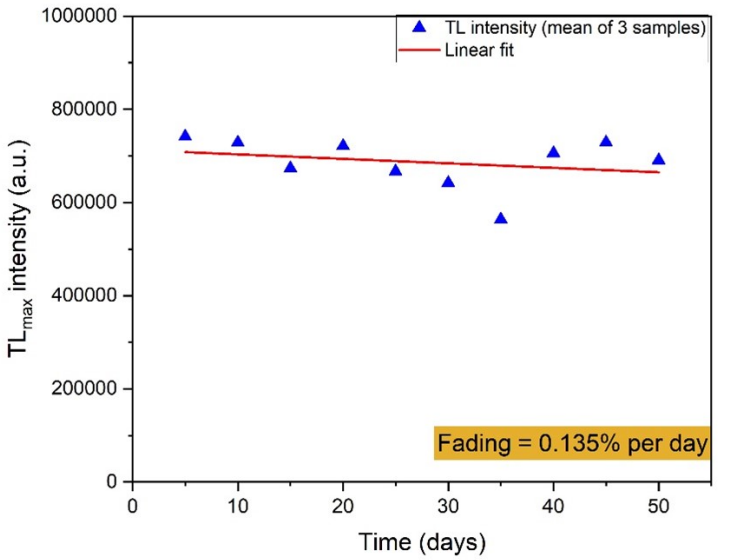

Figure 4.17. TL_max intensity as a function of time. A linear regression curve with fading per day is also given.

$$Fading = \frac{Slope}{Intercept} \times 100\%$$

From figure [4.17], slope of the curve = 964.18, intercept = 713100.08. Therefore,

$$\begin{aligned} Fading &= \frac{Slope}{Intercept} \times 100\% \\ &= \frac{964}{713100} \times 100\% \\ &= 0.135\% per \quad day \end{aligned}$$

Hence, at the end of 50 days fading would be $50 \times 0.135\% = 6.75\%$.

4.8 EPR dosimetry

An experiment was performed to find the response of an irradiated sample of Eu activated $BaSO_4$ as an EPR dosimeter. Before the actual irradiation, calibration for 225 kV X-rays was done, and the dose rate was determined at the source to detector distance (50 cm). Now, a sample of 30 mg phosphor was prepared, and every three samples were irradiated by 1 Gy, 2 Gy, and 3 Gy doses, respectively. These samples were stored in the dark for 24 hours, and then the responses materials were investigated in the magnetic field.

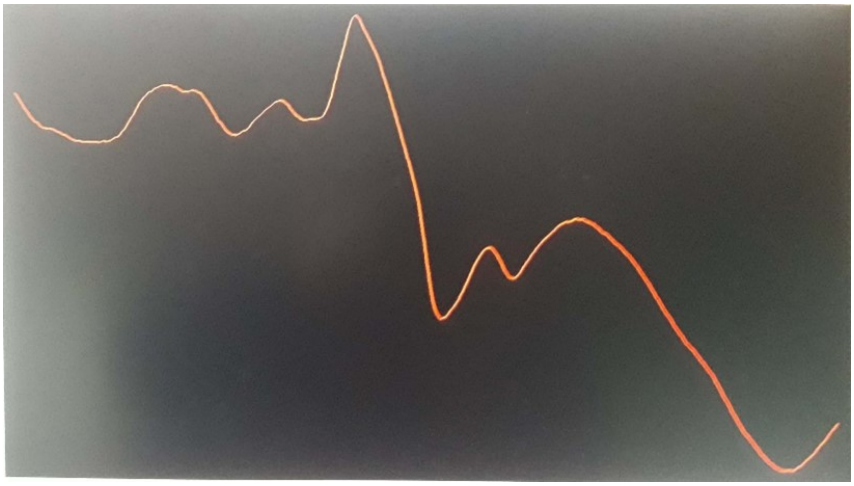

Figure 4.18. EPR signal obtained as a function of magnetic field strength for Eu activated $BaSO_4$ at a dose of 3 Gy (screenshot).

The EPR signal observed is shown in figure [4.18]. In the figure the splitting of

energy levels can be seen as a sharp decrease in EPR signal, and it is energy difference between two splitting levels indicated by peak-to- peak value in figure. The dosimeter data obtained were plotted as peak-to-peak value of EPR signal vs dose, and a linear fit is shown in figure [4.19].

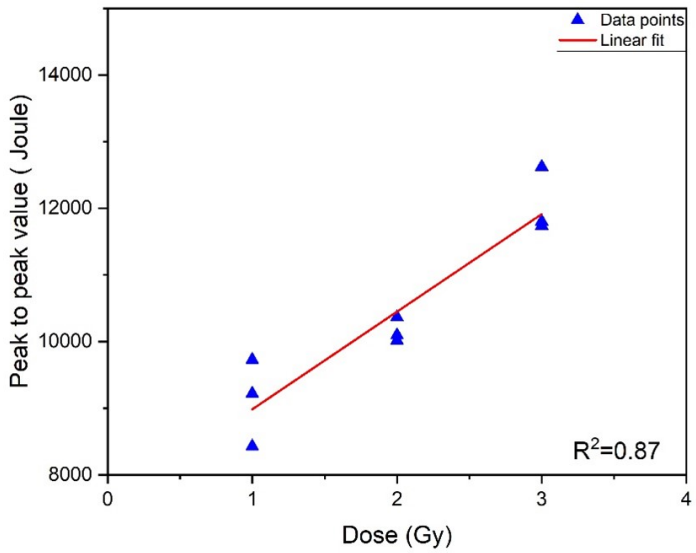

Figure 4.19. Peak-to-peak value of energy as a function of dose. A linear regression curve with goodness of fit (R^2) is also given.

From the above plot, it seems that number of paramagnetic species in the samples increases with the dose. Therefore, there is a nearly linear relationship between dose and EPR intensity with goodness of fit is $R^2 = 0.87$.

Chapter 5

Discussion and Conclusion

It doesn't matter how beautiful your theory is, it doesn't matter how smart you are. If it doesn't agree with experiment, it's wrong.

RICHARD P. FEYNMAN

5.1 Methodology and uncertainties

Thermoluminescence materials are highly sensitive to ionizing radiation after the addition of impurities. The material used for this project work was $BaSO_4$ with the activator Eu (Europium). The material was tested with different concentrations of impurity, and at 0.5 mol % of Eu the maximum sensitivity towards ionizing radiation was found. The material was prepared by co-precipitation method. Besides the co-precipitation method, other methods like the crystalline method, solid-state method, and combustion method may have been employed. Many samples were prepared for different tests and irradiation with X-rays and gamma rays of different masses. For most of the tests, 10 mg of samples were used.

The polycrystalline $Eu : BaSO_4$ has an effective atomic number almost seven times higher than the water as well as human tissue. The dosimeter signal (e.g., TL maximum intensity) is highly dependent on the mass of the sample. As the sample mass is tiny, it is challenging to maintain uniformity to all the samples. There is always a possibility for a slightly different mass in each sample. The uncertainties while preparing the samples leads to varying dosimeter signals for the same absorbed dose. We did indeed see slight variations in TL intensity during the TL measurements, briefly discussed later in this chapter.

Moreover, there is a high probability of loss of a tiny mass of irradiated sample while transferring to the TLD cube system sample holder. The sample size is itself small, so it requires very careful handling. The small particle size of phosphor makes it more vulnerable to stick on the micro-tube vial due to electrostatic attraction.

Besides the uncertainties in the sample size and subsequent dose measurement, thermoluminescence techniques have other drawbacks. One drawback is that it is impossible to get information about the type of radiation by which phosphor is irradiated. The non-uniform distribution of nano-crystalline TL powder over the surface of reader tray and effects due to exposure of material to natural or artificial light can also cause error in the results.

The uncertainties in methodology lead to some of the study limitations in the project. The thermoluminescence phosphor showed a fluctuating TL readout for the same experiments performed in two different periods. Due to this, we had to make some corrections between two experiments. The non-uniform mass of the phosphor sample could be a reason for this fluctuation. The result could have been different if the pellets of nano-crystalline phosphor were used instead of powder. We have studied TL characteristics of $BaSO_4 : Eu$ by taking doses over a small range, and it would be better if we had more dose points instead of having only three points. It would be interesting to study the TL characteristics for a wider range of X-ray spectra. These study limitations will restrict the conclusions of the current work.

5.2 Other studies

Many scholars have investigated the thermoluminescence property of nano crystalline $BaSO_4 : Eu$ phosphor in different aspects. For example, the method of $BaSO4 : Eu$ phosphor preparation, sensitivity with type of ionizing radiation and TLD properties like linearity in dose-response, residual analysis, fading, sensitivity with temperature, and reusability have been investigated. The following table summarizes work on $BaSO4 : Eu$ by different scholars. The results from these studies will be compared to our findings when relevant in the following Table [5.1].

5.3 Linearity

For ideal dosimeter, the reading given by it should be linearly proportional to the absorbed dose. However, beyond certain dose range a non-linearity could be observed [3]. Sharma R *et al.* (2015)[29] reported that nanocrystalline barium sulphate doped with europium prepared by co-precipitation method with the concentration of 0.2 mol% of dopant gives a linear TL response for exceptionally wide range of doses from 10 Gy to 2 kGy of Co-60 gamma radiation having average energy of 1.25 MeV. Lochab *et al.* (2008) [27] have reported that pellets of $BaSO_4 : Eu$ were exposed to ion beams Li^{3+} and Ag^{12+}. They used 48 MeV Li, 150 MeV Ag ion and γ-rays of 137Cs and observed a linearity in the TL response over a wide ranges of particle fluences (scales with absorbed dose). Asfora *et al.* (2021)[26] reported that nano-crystalline BaSO4:Eu showed a linear dose response in the range of 2 mGy to 60 mGy when irradiated with 137Cs γ-rays. Jose *et al.* (2012) [24] have repoerted that polycrystalline barium sulphate dopped with europium shows the linear dose response upto the dose range of 1000 Gy. Beyound which the saturation in linearty for the C0-60 gamma rays.

In this project, the thermoluminescence phosphor $BaSO_4 : Eu$ was irradiated with 1.25 MeV (average energy) gamma rays of a Co-60 source and X-rays of different

TABLE 5.1. Comparative studies made by different scholars.

S.N	Studied by	Method of preparation and concentrationof dopant	Linearity range	Fading	Sensitivity
1	Jose *et al.* (1999)[24]	Co-precipitation	Sublinear dose response in the range 0.5 mGy to 100 Gy.	40% in 40 days	2-3 times higher than that of CaSO4:Dy
2	Raheja *et al.* (2017)[25]	Coprecipitation with 0.2 mol%	10 Gy to 2 kGy	-	28.52 times TLD-100 and 1.426 times TLD-900
3	Asfora *et al.*[26]	Combustion solid state	2mGy to 60mGy	-	5.8 times $CaF_2 : Tm$
4	Lochab *et al.* (2008)[27]	Pallets of $BaSO_4$	Fluence of 10^9 to 10^11 for 48 MeV Li and 10^9 to 10^10 for 150 MeV Ag ions	-	0.374 times relative to 0.662 MeV γ-rays for 48MeV Li and 0.0017 times relative to 0.662MeV γ-rays for 150MeV Ag ions.
5	González *et al.* (2007)[28]	Crystallization technique with 0.5 mol%	0.05 mGy to 50 Gy with Co-60 source	-	-
6	Furetta *et al.* (1991)[5]	Sheet of $BaSO_4 : Eu$ embedded in polytetrafluoroethylene	4 mGy to 50 Gy with Co-60 source	-	3-4 times than $CaSO_4 : Dy$.

voltages like 100, 160, and 225 kV. The dose response (TL intensity vs dose) was investigated qualitatively by inspecting the glow curves and quantitatively by linear regression. From the regression, we found R^2 values of typically 0.95, pointing to that around 95 % of the response may be explained by the linear relationship. The remaining 5 % may be due to the uncertainties related to mass of the sample, which may lead to the variations in the TL intensities. The TL response was observed to be linear for γ-rays in the dose range 0.1 Gy to 1 Gy at 10 different dose levels. Similar

results were also observed with X-rays at different energies with dose of 0.1 Gy to 0.3 Gy.

EPR dosimetry was also performed by irradiating phosphors with the dose range from 1 to 3 Gy by 225 kV X-rays. The splitting of energy levels in the strong magnetic field was observed in the form of an EPR signal. A linear relationship was observed between the intensity of the peak-to-peak signal and dose.

5.4 Heating rate and residuals

In this work, the heating rate effect and residuals present after heating the sample of nanocrystalline $BaSO4 : Eu$ was studied. The sample was irradiated with a dose of 0.01 Gy by 225 kV X-rays. With the increase in the heating rate from 5 K/s to 20 K/s, the TL intensity increased with the shift of the TL peak towards higher temperature. Since the dose in the sample was same, the increase in TL intensity is due to the rapid movement of electrons in the conduction band. According to Randall-Wilkin's theory, for a constant dose, as the heating rate increases the TL glow peak increases gradually, which can be seen in equation [2.22]. The electrons in the electron trap are released into conduction band if the temperature of the sample rises. The electrons in the conduction band can either recombine with holes at the recombination center (RC) or be trapped in the electron trap. Also, when heating rate changes, there is a shift of the TL peak towards higher temperature side. Although there was a linear increase in TL intensity with heating rate, the area under the curve was found to decrease as the heating rate increases.

The residuals are then tested, and it was observed that as the heating rate increases, the residual signal also increases. With high heating rate, the electros in the deep traps cannot escape out to the conduction band, remains in the traps there by increases the residual signal.

5.5 Reusability and fading

The reusability and fading are very important features of a dosimeter material. To reuse a TL dosimeter, it needs to be annealed. The annealing is the process to remove all the residual signals present in the material. Different materials have different annealing temperature and reading/annealing procedures. By annealing the trapped electrons may be removed but may at the same time cause thermal damages to the phosphors that cause addition of unwanted background signals during reuse.

The inability of a material to retain the trapped charges in the electron traps is called fading. Due to fading the thermoluminescence material lose TL signal gradually. It depends upon the depth of the electron traps in the meta-stable state.

González *et al*.[28] have reported that pellets of $BaSO_4 : Eu$ were given a test dose of 264 mGy. They used ten pellets for irradiation by Co-60 source for ten annealing cycles. First, the samples were irradiated, and readouts were taken, followed by annealing. Then, the exact process continued for ten consecutive cycles. The reproducibility parameter they took was the percentage standard deviation, which they reported to be 2.04 %. Madhusoodanan *et al*.[24] reported that the phosphor was irradiated by γ-rays with a dose of 1 Gy and stored at room temperature. Fading was observed for an interval of 40 days. They observed nearly 40 % of fading in TL intensity. Raheja *et al*. (2017) have reported that reproducibility parameter for nanocrystalline $BaSO_4 : Eu$ tested for 10 cycles and they found repeatability of 2.76 %, which was below the acceptable value of 7.5 %.

For this work, the reusability test was performed by irradiating the material with a dose of 0.01 Gy by 225 kV X-rays. The reusability was observed for ten different cycles of irradiation followed by storing for 24 hours, readout, and finally annealing. It was observed that after the first cycle of readout, there was a decrease in the TL intensity or sensitivity of the material, followed by a nearly stable readout for the remaining cycles. The reusability or reproducibility parameter was calculated for all ten cycles,

and it was found to be 1.20. The same value was also calculated for the last nine cycles, excluding the first cycle, and it was found to be 0.336. These values of the reproducibility parameter are well inside the acceptance value of 7.5 %, so the material has good reproducibility for dosimetric applications. When the phosphor is heated at a high temperature, the increase in thermal vibrations will cause increase in the rate of release of trapped electrons. When the phosphor is heated above 300 $^{\circ}C$, the thermal energy may cause a change in the molecular structure, reducing the number of traps in the molecule[30]. Since the phosphor was annealed at 400 $^{\circ}C$, the decrease in TL sensitivity may be expected after the first annealing cycle because of permanent decrease in the number of traps in the molecule after annealing.

For fading, the samples were irradiated by Co-60 source with a dose of 0.5 Gy. The samples were stored at room temperature in a dark atmosphere to avoid any exposure to UV or any other light exposure. With the 50 days of storage time, the fading of TL material was observed to be 6.75 %. The fading of the TL material can be expected as the shallow traps are unstable and releases electron from it to the conduction band. It is caused by combined effect of thermal, mechanical, and optical stimulation of charge carriers and these factors are difficult to control in natural environment [31].

5.6 Energy dependence

One of the properties of the good dosimeter material is that it must be energy independent. Pandey *et al.*[29] have reported that they prepared two groups of nanocrystalline $BaSO_4 : Eu$, in which one group was irradiated with a dose range of 10 Gy to 300 Gy by a Co-60 source (mean energy 1.25 MeV) while the other group was irradiated with a dose range of 1 Gy to 300 Gy by Cs-137 gamma of energy 662 keV. They observed that the shape of the glow curve remained similar for overlaping dose ranges and also, with changing the energy and source of gamma radiation, there shows little variation in TL response. They reached to a conclusion that nanocrystalline $BaSO_4 : Eu$ is an energy independent dosimeter.

However, in my present work, the results are different. The sensitivity of the material was compared between the two different types and energy of radiations. The TL response of the material was compared between X-rays and γ-rays. The X-rays are the spectrum of different energies (polyenergetic) and γ-rays are monoenergetic photon beam with much higher mean energy. The X-ray voltages used were 100 kV, 160 kV and 225 kV and the Co-60 source (γ-rays) has 1.25 MeV average energy. During the interaction of ionizing radiation to a matter, the photoelectric effect is dominant at lower photon energies and high atomic number of the absorbing material. From a few hundred keV to several MeV photon energy, the Compton Effect plays dominant role. Since the average atomic number of $BaSO_4$ is 46.9 and the energy of X-rays used was low compared to γ-rays, the deposition of energy in the dosimeter is dominated by photoelectric effect. Also, the energy deposition in a matter is proportional to mass energy absorption coefficient, which is evident in figure [4.10] (relative to water). Here, it appears that the $BaSO_4$ is energy independent above approximately 400 keV. Experimentally, the TL sensitivity of $BaSO_4$ with x-rays of energies 100, 160 and 225 kV was found to be 47, 49 and 63 respectively relative to Co-60 γ-rays. Thus, the current work demonstrates that $BaSO_4$ is strongly dependent on photon energy in the X-ray energy domain (< 225 keV).

5.7 Conclusion

Nano-crystalline $BaSO_4 : Eu$ was prepared by co-precipitation method, in which $BaCl_2$ was dissolved in $EuCl_2$ and $(NH_4)_2SO_4$ in deionized water. The phosphor was prepared by choosing the concentration of dopant so that it would give maximum sensitivity towards the ionizing radiation. The optimum concentration of the europium was found to be 0.5 mol %. The precipitates of Eu activated barium sulfate was first dried in an oven at 100 $^\circ C$ for 2 hours, and it was ground in fine powder and annealed at 850 $^\circ C$ for 1 hour under nitrogen atmosphere. By annealing it before actual irradiation is to release all the prior stored energy and increase the sensitivity of the phosphor.

The irradiation of phosphor was done by two different types and energy of the photons to study the material's behavior in different radiations. The glow curve plotted as a function of temperature and TL intensity, contains two glow peaks, the main peak was observed at a temperature around 225 $^{\circ}C$, and another peak was observed around 325 $^{\circ}C$. The temperature of glow peaks was found almost the same in both X-rays and γ-ray. Hence, similar glow curves were observed for both types of radiations. A linear relationship was observed between the dose and TL peak intensity in the range of 0.1 Gy to 1 Gy of γ-radiations having average energy of 1.25 MeV. A similar association was observed for X-rays of a dose range 0.1 Gy to 0.3 Gy for the spectrum energies of 100 kV, 160 kV and 225 kV.

The TL sensitivity of the material was found nearly equal for X-rays at energies 100 kV and 225 kV. However, it was observed that the sensitivity of X-rays at 225 kV was 47 times the sensitivity of γ-rays of average energy 1.25 MeV. To compare the theoretical calculations with experimental results, the calculated dose deposition in $BaSO_4$ by X-rays of the same energy was found to be 41 times higher than the dose deposited by γ-rays by the corresponding energy. This shows the theoretical and experimental results are quite close to each other. In the plot between ratio of mass attenuation coefficients of $BaSO_4$ and water and photon energy, it was of interest to find an energy of X-rays which have higher sensitivity than at 100 kV and 225 kV. The new energy was found to be 160 kV, at which $BaSO_4$ was 63 times more sensitive than γ-rays. These results confirm the energy dependency of nano-crystalline phosphor.

The heating rate effect was observed in phosphors by irradiating with X-rays. Different heating rates like 5, 10, 15 and 20 K/s were applied. The shift in the glow curve peak was observed towards the higher temperature. A linear relation was observed between the dose and TL maximum intensity. The peak temperatures 224 $^{\circ}C$, 240 $^{\circ}C$, 254 $^{\circ}C$ and 270 $^{\circ}C$ were marked for heating rates of 5, 10, 15 and 20 K/s. With the increase in heating rates, the second peak in the glow curve tends to vanish. The residual test was performed to test the residual signal present in the sample after different heating rates. The increase in residual was observed with an increase in heating rate, due to which the second peak in the glow curve vanishes at a higher

heating rate. The deep traps are unaffected by a higher heating rate, due to which the residual signals increase with the increase in heating rate.

The reusability of a dosimetry material is one of the most important properties, especially in TLDs. The reusability was studied by irradiating the nano-crystalline phosphor by X-rays, followed by TL measurement, and finally annealing at 400 $^{\circ}C$ for 30 minutes. This process was repeated for ten consecutive cycles. During TL measurement, the constant heating rate of 5 K/s was applied. After the first cycle, the decrease in TL intensity was observed, followed by almost stable TL intensity for the rest of the consecutive cycles.

The fading of $BaSO_4$ was studied under the irradiation by γ-rays with 0.5 Gy dose. The TL measurement of the samples was done in the interval of five days for ten cycles and in a total of 50 days duration. The negative slope of the linear regression curve shows there was a decrease in the TL signal. There was also a pronounced drop in intensity after the first cycle. The fading in the TL signal was less than 7 % in 50 days. This indicates the material has significantly less fading even after a prolonged storage period.

Moreover, EPR dosimetry was also performed to observe the relation between EPR peak to peak intensity with dose. X-rays of energy 225 kV irradiated 30 mg phosphor with doses 1 Gy, 2 Gy and 3 Gy. When the phosphor was analyzed with EPR, it was observed that there was a linear relationship was observed between the number of radicals and dose.

In conclusion, nanocrystalline $BaSO_4$ material has good thermoluminescence properties, making it useful for medical research dosimetry applications. Still, the high X-ray sensitivity may limit the applicability for photon energies below approximately 400 keV.

5.8 Direction for future work

In this work, the nanocrystalline phosphor was irradiated with X-rays and γ-rays, although it was tested for only few X-ray voltages like 100 kV, 160 kV and 225 kV. As from this study it was observed that different X-ray voltages give different dosimeter sensitivities. The following are some recommendations for further work.

In the future, it would be of relevance to:

- Study how the phosphor behaves for a wider range of X-ray voltages.
- Investigate its behavior with heavy ion beams like protons, lithium ions, carbon ions etc.
- Study the thermoluminescence of barium sulfate by using different dopants/co-dopants and varying their concentrations.
- Look deeper into the TL emission spectra of the phosphor, possibly to better appraise the radiation quality
- Perform a comparative study of the $BaSO_4$ material with standard thermoluminescence materials like LiF: Mg,Ti ('TLD-100').

Appendix A

Irradiation of $BaSO_4$: Eu with X-rays

Nanocrystalline $BaSO_4 : Eu$ was irradiated with 100, 160, and 225 kV X-rays. The dose range of irradiation was from 0.01 Gy to 0.03. The sample phosphor was rested for 24 hours after irradiation. The thermoluminescence of the phosphor can be studied by using a TLD reader cube. The output given by the TLD reader was plotted as a glow curve between TL intensity as a function of the measured temperature, as shown in figure [A.1]. The different colored glow curve is plotted for different doses. For example, the black colored curve for a dose of 0.01 Gy, red for 0.02 Gy, and Blue for 3 Gy doses. The glow curve was the mean curve of all the sample data (3 samples). The increase in the intensity was observed with the increase in the doses from 0.01 Gy to 0.03 Gy. Similarly, for 225 kV X-rays, a glow curve was plotted between TL intensity and measured temperature, as shown in figure [A.3]. The increase in the TL intensity with an increase in dose was observed for the dose range from 0.01 Gy to 0.03 Gy. The glow curve was also plotted for 160 kV for the same dose range; the increase in TL intensity with the increase in dose was observed, shown in figure [A.5].

The glow curve of nanocrystalline phosphor $BaSO_4 : Eu$ shows two peaks. The relationship between the peak intensity with dose was observed by plotting a curve between Maximum peak intensity for second peak and dose. A linear regression curve was plotted between second peak maxima and dose, as shown in figure [A.2]. A linear

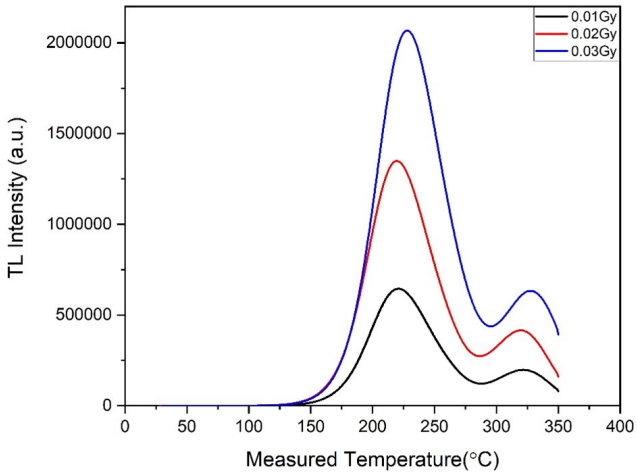

Figure A.1. Glow curve between TL intensity and measured temperature for 100 kV X-rays.

relation was observed with the value of goodness of fit 0.95.

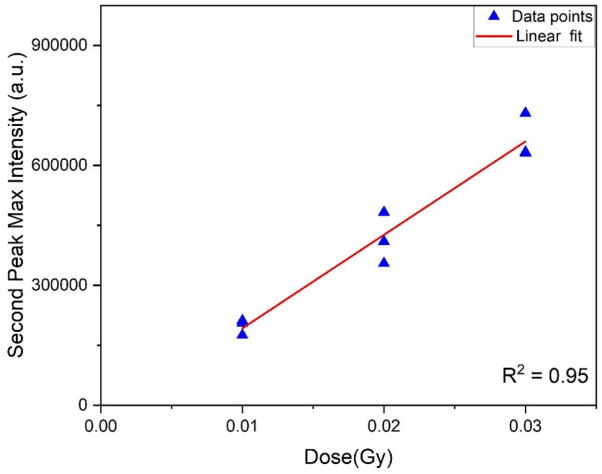

Figure A.2. Second peak maximum intensity versus dose linear regression curve for 100 kv X-rays. The goodness of fit (R^2) is given.

Figure [A.4] shows a linear regression curve between the area under the curve and doses. A linear relationship between area under the curve and doses was observed with goodness of fit $R^2 = 0.95$.

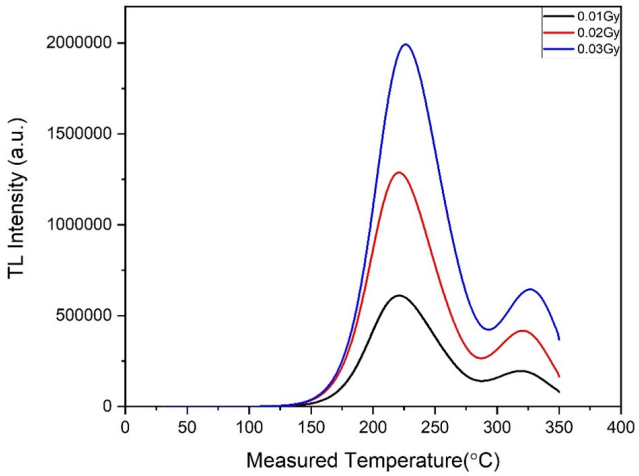

Figure A.3. Glow curve between TL intensity and measured temperature for 225 kV X-rays.

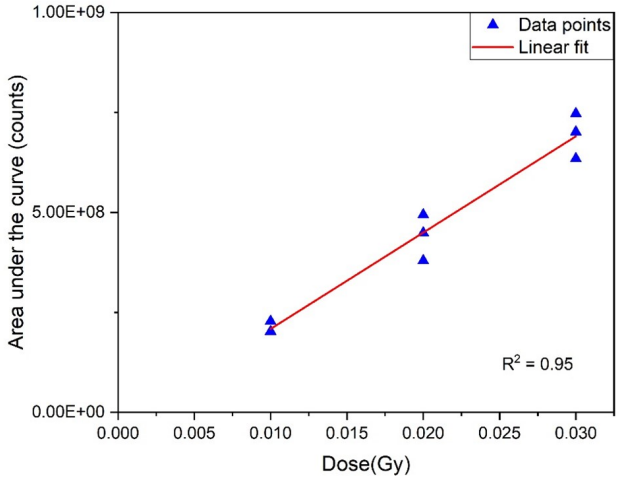

Figure A.4. Area under the curve versus dose linear regression curve for 225 kV X-rays. The goodness of fit (R^2) is given.

The linear regression curves between TL_{max} intensity and doses were plotted as the mean of three samples for 100, 160, and 225 kV X-rays. The slope of the linear regression curve gives the sensitivity of the material with corresponding X-rays potentials. Figure [A.6] shows that the linear regression curve for 100, 160, and 225 kV was represented by blue, black, and red lines, respectively. The sensitivity for 100 and 225 kV X-rays are found to be similar; however, the sensitivity of 160 kV X-rays was found to be 23 % higher than that for 225 kV X-rays. So, the highest sensitivity was observed at 160 kV compared to 100 and 225 kV for the given phosphor.

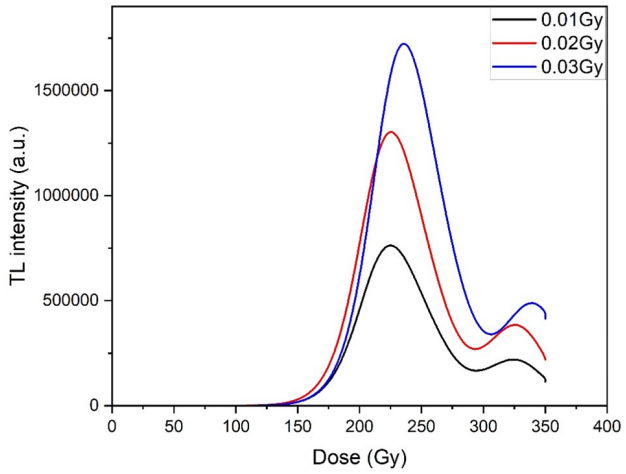

Figure A.5. Glow curve between TL intensity and measured temperature for 160 kV X-rays.

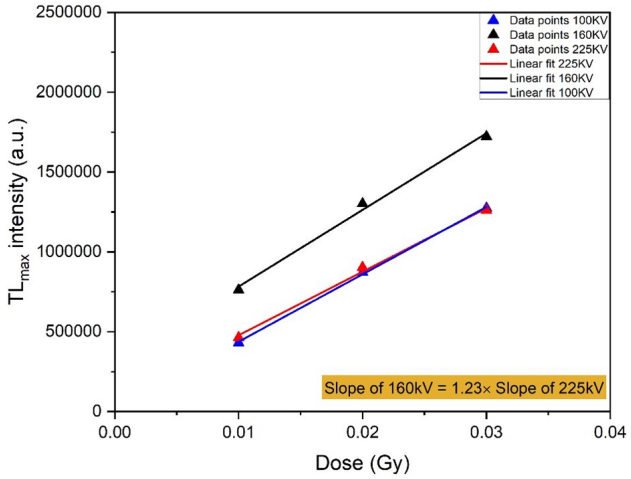

Figure A.6. TL max intensity versus dose for 100 kV, 160 kV and 225 kV for X-rays with compared slopes of 160 kV and 225 kV X-rays.

The reusability of the phosphor was performed by irradiating a sample by a dose of 0.01 Gy with 225 kV X-rays. The sample was rested for 24 hours after irradiation, followed by TL measurement for reusability. The sample was annealed after the first cycle and irradiated again. The same process was repeated for ten consecutive cycles. The mean of all data was plotted between TLmax intensity and the number of cycles, as shown in figure [A.7].

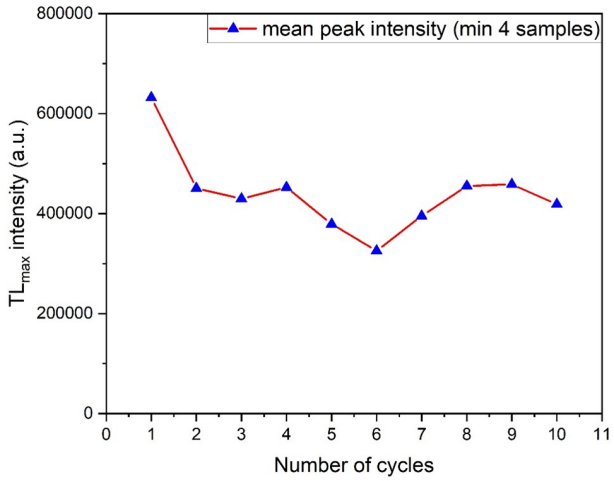

Figure A.7. (Reusability test) TL maximum intensity vs. number of cycles plot.

Bibliography

[1] Bruce Alberts et al. 'Molecular biology of the cell'. In: *SCANDINAVIAN JOURNAL OF RHEUMATOLOGY* 32.2 (2003), pp. 125–125.

[2] William R Hendee, Geoffrey S Ibbott and Eric G Hendee. *Radiation therapy physics*. John Wiley & Sons, 2013.

[3] Ervin B Podgorsak et al. *Radiation oncology physics.* IAEA Vienna, 2005.

[4] Alastair F McKinlay. 'Thermoluminescence dosimetry'. In: (1981).

[5] Claudio Furetta. *Handbook of thermoluminescence*. World Scientific, 2010.

[6] Stephen WS McKeever, Marko Moscovitch and Peter David Townsend. 'Thermoluminescence dosimetry materials: properties and uses'. In: (1995).

[7] Reuven Chen and Stephen WS McKeever. *Theory of thermoluminescence and related phenomena*. World Scientific, 1997.

[8] Yigal S Horowitz. *Thermoluminescence and thermoluminescent dosimetry*. Vol. 1. CRC Press Boca Raton, 1984.

[9] Frank Herbert Attix. *Introduction to radiological physics and radiation dosimetry*. John Wiley & Sons, 2008.

[10] Boualem Djezzar. *Ionizing Radiation Effects and Applications*. BoD–Books on Demand, 2018.

[11] Rita Joana da Cruz Roque. 'X-ray imaging using 100 μm thick Gas Electron Multipliers operating in Kr-CO2 mixtures'. PhD thesis. Universidade de Coimbra, 2018.

[12] Motohiro Uo, Takahiro Wada and Tomoko Sugiyama. 'Applications of X-ray fluorescence analysis (XRF) to dental and medical specimens'. In: *Japanese Dental Science Review* 51.1 (2015), pp. 2–9.

[13] Raja Aamir Younis. 'Using MARS spectral CT for identifying biomedical nanoparticles'. In: *University of Canterbury, New Zealand* (2013).

[14] JOANNA Izewska and Govinda Rajan. 'Radiation dosimeters'. In: *Radiation oncology physics: A Handbook for teachers and students* (2005), pp. 71–99.

[15] Carlo Corvaja. 'Introduction to electron paramagnetic resonance'. In: *Electron Paramagnetic Resonance*. 2008.

[16] *Centrifuges, bench top, ventilated/refrigerated, Mega Star 600 / 600R*. URL: https://uk.vwr.com/store/product/13993719/centrifuges-bench-top-ventilated-refrigerated-mega-star-600-600r.

[17] *FC65-G / FC65-P ionization chambers*. URL: https://www.iba-dosimetry.com/product/fc65-g-fc65-p-ionization-chambers/.

[18] Pedro Andreo et al. 'Absorbed dose determination in photon and electron beams. An international Code of Practice'. In: (1987).

[19] *Max 4000 plus electrometer*. URL: https://www.standardimaging.com/electrometers/max-4000-plus-electrometer.

[20] *Luminescence measurement devices*. Feb. 2021. URL: https://www.lexsyg.com/tlosl-reader.html.

[21] *Muffle furnaces up to 1100°C or 1200°C*. URL: https://nabertherm.com/en/products/laboratory/muffle-furnaces/muffle-furnaces-1100-degc-or-1200-degc.

[22] Curtis.suplee@nist.gov. *X-ray mass attenuation coefficients*. Dec. 2019. URL: https://www.nist.gov/pml/x-ray-mass-attenuation-coefficients.

[23] S Del Sol Fernández et al. 'Thermoluminescent characteristics of LiF:Mg, Cu, P and CaSO4:Dy for low dose measurement'. In: *Applied Radiation and Isotopes* 111 (2016), pp. 50–55. ISSN: 0969-8043. DOI: https://doi.org/10.1016/j.apradiso.2016.02.011. URL: https://www.sciencedirect.com/science/article/pii/S0969804316300756.

[24] U Madhusoodanan, M T Jose and A R Lakshmanan. 'Development of BaSO4:Eu thermoluminescence phosphor'. In: *Radiation Measurements* 30.1 (1999), pp. 65–72. ISSN: 1350-4487. DOI: https://doi.org/10.1016/S1350-4487(98)00083-3. URL: https://www.sciencedirect.com/science/article/pii/S1350448798000833.

[25] A Pandey et al. 'Nanocrystalline Europium doped barium sulphate as an energy independent thermoluminescent dosimeter'. In: *AIP Conference Proceedings* 1832.1 (2017), p. 50034. DOI: 10.1063/1.4980267. URL: https://aip.scitation.org/doi/abs/10.1063/1.4980267.

[26] Taqmeem Hussain et al. 'Thermoluminescence properties of nanocrystalline BaSO4 doped with Eu2+ produced by solid state combustion synthesis'. In: *Radiation Physics and Chemistry* 186 (2021), p. 109531. ISSN: 0969-806X. DOI: https://doi.org/10.1016/j.radphyschem.2021.109531. URL: https://www.sciencedirect.com/science/article/pii/S0969806X2100181X.

[27] Numan Salah et al. 'Thermoluminescence of BaSO4: Eu irradiated with 48 MeV Li3+ and 150 MeV Ag12+ ions'. In: *Journal of Physics D: Applied Physics* 41.8 (2008), p. 085408.

[28] P R González et al. 'Dosimetric characterization of a new preparation of BaSO4 activated by Eu ions'. In: *Nuclear Instruments and Methods in Physics Research Section B: Beam Interactions with Materials and Atoms* 260.2 (2007), pp. 685–692. ISSN: 0168-583X. DOI: https://doi.org/10.1016/j.nimb.2007.04.155. URL: https://www.sciencedirect.com/science/article/pii/S0168583X07009615.

[29] Anant Pandey et al. 'Radiation dosimetry using nano-BaSO_4: Eu'. In: (2015).

[30] TNH Tengku Kamarnl Bahri, R Hussin and NE Ahmad. 'The influence of annealing temperature and heating rate on thermoluminescence properties of nanocrystalline calcium borate powder'. In: *EPJ Web of Conferences*. Vol. 156. EDP Sciences. 2017, p. 00010.

[31] Ravikumar Nattudurai et al. 'Thermoluminescence characteristics of biological tissue equivalent single crystal: europium doped lithium tetraborate for dosimetry applications'. In: *Journal of Materials Science: Materials in Electronics* 29.17 (2018), pp. 14427–14434.